# Investigation of Thermal Buffer Zone Effectiveness in Real Buildings

# Investigation of Thermal Buffer Zone Effectiveness in Real Buildings

By

Abdulrahman M. Almansour, BS Mechanical Engineering

A Thesis

Submitted to the School of Graduate Studies

In Partial Fulfillment of the Requirement

For the Degree

Master of Applied Science

McMaster University

Hamilton, Ontario, Canada

© Copyright by Abdulrahman M. Almansour, October 2018

MASTER OF APPLIED SCIENCE (2018) McMaster University

(Mechanical Engineering) Hamilton, Ontario

TITLE: Investigation of Thermal Buffer Zone Effectiveness in Real Buildings

AUTHOR: Abdulrahman M. Almansour, BS Mech. Engineering

SUPERVISOR: Dr. Mohamed S. Hamed

NUMBER OF PAGES: 81

## Abstract

Global warming is caused by Greenhouse Gas (GHG) emissions produced from the use of fossil fuel-based energy sources. Buildings consume about 30%-35% of the global energy use, which makes buildings a major contributor to the global warming problem. A long-term plan has been established at the Thermal Processing Laboratory (TPL) at McMaster University to investigate the use of various renewable energy-based technologies to achieve Net-zero energy buildings in Canada. This thesis presents results of an investigation of the effectiveness of using a thermal buffer zone (TBZ) in real buildings. A TBZ is a closed passage built around the building that allows air to passively re-distribute heat energy from solar radiation received on the south side throughout the building. A TBZ offers an effective solution of the overheating problem usually experienced on the south side of the building and, at the same time, it helps in reducing the heating load of the north side of the building. An experimental setup employing TBZ in a model of a typical building floor has been built. An analytical model of the TBZ has been developed. The experimental data has been used to validate the developed analytical model, which then was used to simulate the performance of a TBZ implemented in a real building floor. Results showed that the effectiveness of TBZ could reach 117% in the winter (cold climate countries) and 72% in the summer (hot climate countries). Moreover, the study considered the effect of integrating the TBZ with a fan. Results showed that the use of the fan is beneficial for a certain gap width, beyond which the use of the fan is not recommended. In

conclusion, results of this study confirm that the TBZ can offer an effective means of replacing parry of building consumption of fossil fuel-based energy using solar energy.

## Acknowledgements

I would like to take this opportunity to thank my supervisor Dr. Mohamed S. Hamed, for his guidance, advice, and support throughout the project. Also, I would like to thank all the technicians in the department, John and Justin for their help and advice. I would also like to acknowledge the group of undergraduate students for their help in the reconstruction the experimental setup.

Finally, I would like to thank my family for their support during the past two years that made this achievement possible.

# Table of Contents:

## List of Tables:

## List of Figures:

## List of Symbols:

| SYMBOL | DESCRIPTION | UNITS |
|---|---|---|
| $A$ | Cross-section area of the cavity | $m^2$ |
| $A_n$ | Calibration coefficient | $\frac{1}{V}$ |
| $A_s$ | Surface area | $m^2$ |
| $B$ | Spacing between glass plates | $m$ |
| $C_p$ | Specific heat capacity | $\frac{J}{kg\,℃}$ |
| $D_H$ | Dynamic diameter | $m$ |
| $e$ | Measured voltage | $V$ |
| $f$ | Frictional coefficient | $-$ |
| $f(\,)$ | Manufacturer provided calibration function | $-$ |
| $g$ | Gravitational acceleration | $\frac{m}{s^2}$ |
| $h$ | Convection heat transfer coefficient | $\frac{W}{m^2\,℃}$ |
| $h_f$ | Forced convection heat transfer coefficient | $\frac{W}{m^2\,℃}$ |
| $h_L$ | Total head loss | $m$ |

| | | |
|---|---|---|
| $h_l$ | Major head loss | $m$ |
| $h_{lm}$ | Minor head loss | $m$ |
| $h_n$ | Natural convection heat transfer coefficient | $\frac{W}{m^2\,℃}$ |
| $H$ | Total cavity height | $m$ |
| $k$ | Thermal conductivity | $\frac{W}{m\,℃}$ |
| $K$ | Loss coefficient | $-$ |
| $K_{add}$ | Additional loss coefficient | $-$ |
| $L$ | Spacing between interion glass and illumination | $m$ |
| $\dot{m}$ | Mass flow rate | $\frac{kg}{s}$ |
| $Nu_{D_H}$ | Nusselt number based on dynamic diameter | $-$ |
| $P$ | Measured atmospheric pressure | $Pa$ |
| $P_{drive}$ | Driving pressure | $Pa$ |
| $P_{drop}$ | Pressure drop | $Pa$ |
| $Pr$ | Prandtl number | $-$ |
| $q$ | Heat flux | $\frac{W}{m^2}$ |

| | | |
|---|---|---|
| $Q_{inc}$ | Incident heat flux | $\frac{W}{m^2}$ |
| $Q_{TBZ}$ | Heat enter the room with using TBZ | $W$ |
| $Q_{W/O}$ | Heat enter the room without using TBZ | $W$ |
| $r$ | Relative humidity | $\%$ |
| $R$ | Ideal gas constant | $\frac{J}{mol.\ K}$ |
| $R_c$ | Thermal conduction resistance | $\frac{℃}{W}$ |
| $R_f$ | Thermal forced convection resistance | $\frac{℃}{W}$ |
| $R_n$ | Thermal natural convection resistance | $\frac{℃}{W}$ |
| $Re$ | Reynolds number | $-$ |
| $T$ | Air Temperature in the cavity | $K$ |
| $T_{amb}$ | Ambient Temperature | ℃ |
| $T_N$ | Temperature in North Side of TBZ | ℃ |
| $T_R$ | Room Temperature | ℃ |
| $T_S$ | Temperature in South Side of TBZ | ℃ |
| $T_1$ | Upper South Corner Temperature in TBZ | ℃ |

| | | |
|---|---|---|
| $T_2$ | Upper North Corner Temperature in TBZ | ℃ |
| $T_3$ | Lower North Corner Temperature in TBZ | ℃ |
| $T_4$ | Lower South Corner Temperature in TBZ | ℃ |
| $u( )$ | Uncertainty in ( ) | $-$ |
| $v$ | Velocity | $\frac{m}{s}$ |
| $\bar{v}$ | Area averaged velocity | $\frac{m}{s}$ |
| $V$ | Volume | $m^3$ |
| $W_n$ | $n^{th}$ variable | $-$ |
| $W$ | Weight of the air column | $N$ |
| $\alpha$ | Thermal diffusivity | $\frac{m^2}{s}$ |
| $\beta$ | Thermal expansion coefficient | $\frac{1}{℃}$ |
| $\eta$ | TBZ Effectiveness | % |
| $\upsilon$ | Kinematic viscosity | $\frac{m^2}{s}$ |
| $\mu$ | Dynamic viscosity | $\frac{kg}{m\,s}$ |
| $\rho$ | Density | $\frac{kg}{m\,s}$ |

# Chapter 1

# 1. Introduction

## 1.1 Background

Increasing energy consumption continues to be one of the most important issues facing the world. The majority of the energy consumed world wide comes from non-renewable resources such as coal, natural gas, and petroleum products. Growing economy and population have played a significant role in contributing to a surge in demand for energy, intensifying the environmental impact resulting from energy overuse and making it a more serious concern nowadays compared to the past. Non-renewable sources in particular create much more harm than renewable energy by emitting harmful emissions, e.g., carbon dioxide, and other air and water pollutants. The resulting pollution contributes to global warming, the effects of which include loss of sea ice, accelerated sea level increase, more intense heat waves, stronger hurricanes, and so on. Therefore, there is a greater demand today for more efficient and clean energy use methods.

The building sector accounts for about 30%-35% of the total energy consumption worldwide (International Energy Agency, Buildings, 2017). In cold countries around 45% of the total energy consumption by buildings used for space heating (International Energy Agency, Buildings Overview, 2010). In Canada, due

to the extreme and varying weather during the year, a large proportion of energy use is for heating buildings. In 2015, the building sector in Canada consumed around 60% of total energy consumption (Natural Resources Canada, 2018), which leads to that space heating alone consumed around 18% of the total energy consumed in the country which is mainly from non-renewable resources.

Governments and authorities around the world are committed to reducing the negative impact on the environment by investing and researching more energy-efficient strategies. Many buildings have been designed and built to optimize the use of energy as a result of applying the theory of chimney effects, natural air convection, pressure drop effect, buoyancy effect, and other theories in experiments. The idea of Net Zero Energy Building (NZEB) received more attention in the 1970's due to the high oil prices. NZEB is achieved by replacing fossil fuels with renewable energy. In Canada, Net Zero Energy (NZE) homes are designed to produce as much energy as they consume on an annual basis. Although, the idea is promising, we still have a long way to fully achieve the Net Zero goal.

NZE can be reached by integrating the two following approaches. The first approach is to increase the energy produced by renewable resources, by such active means as utilizing solar energy in photovoltaic electrical generation and wind energy. The second approach is to reduce the buildings' energy consumption with passive methods such as shading, natural ventilation, and air heating. This work explores implementing passive solar air heating in buildings.

## 1.2 Literature Review

As awareness of the impact of non-renewable energy on the environment and economy increased, so did the number of research papers studying passive methods of energy use reduction. This section reviews some of the studies that are relevant to the topic of this work.

### 1.2.1. Passive Solar Air Collector

Onbasioglu & Egrican (2002) implemented an experiment to test the passive solar heating system with a focus on determination of the thermal performance on the black surface wall. The thermal response of the wall, which was similar to Trombe wall without the storage property, was analyzed through temperature, velocity and flux measurements and their acquisition. The result showed that the temperature on the black surface wall was extremely affected by the solar radiation intensity.

Solar Dynamic Buffer Zone (SDBZ) is a simple and low-cost method that uses solar energy to collect heat for the building through the movement of air. The research of Richman & Pressnail (2009) reviewed the conceptual layout of Solar Dynamic Buffer Zone (SDBZ) curtain wall system, which was designed, developed, and tested at the University of Toronto, Toronto, Canada. The study proved that SDBZ curtain wall could provide 90% of the fresh air needed by mid-size commercial building, decreasing the fresh air preheating done by the building's air

handling system. Moreover, Richman & Pressnail (2010) also came up with a validated numerical model that could simulate SDBZ in a building. The numerical model showed high correlation with the experimental data in the case study of the performance of a solar air collector curtain wall reached to 25%-30% efficiency.

Fiuk et al. (2017) and Ryan & Burek (2010) both studied passive solar air collector. A passive solar system could adjust the building temperature using the buoyancy effect and natural convection. Fiuk et al. (2017) set up a transparent, 5mm thick cellular polycarbonate sheet with a range of irradiance G = 0 - 540 W/m2, and concluded that this material achieved thermal efficiency of 36%. Furthermore, Ryan & Burek (2010) carried out an experiment on a prototype passive solar air collector in order to analyze the influence of solar air collector height on mass flow rate and heat transfer. The solar air collector had multiple height settings which are 0.5, 1.0, and 2.0 m with adjustable cavity depths between 20 and 150 mm. By applying multiple heat input values, the study found that thermal efficiency was positively correlated and dependent on the height and heat input whereas it was independent of cavity depth. Moreover, the experiment showed that mass flow rate was dependent on cavity depth, heat input and height of the solar air collector.

### 1.2.2. Solar Chimney

Bouchair (1994) and Chen et al. (2003) studied air flow rate in a solar chimney. Bouchair's paper showed that the air flow rate grew along with channel depth until a depth of 300 mm, beyond which backflow could happen, whereas Chen et al. (2003) examined the ratio of gap width to chimney height and found that the air flow rate increased with the increasing the gap width. Moreover, the study showed that maximum air flow rate occurred when the chimney's incline was at 45° with a gap size of 0.2 m and a height of 1.5 m. The study also showed a relationship between the temperature and velocity uniform distribution and the gap width.

Afonso & Oliveira (2000) worked on a simulation and experiment of the use of solar chimneys in buildings in Porto. The paper illustrates that in the winter in Portugal, solar efficiencies were between 10% and 22%. The result showed that in order to utilize the pattern in buildings operating during the day, thinner chimney walls were recommended, whereas thicker walls were better suited to night operation. However, any increase in wall thickness beyond 10 cm would cause no significant changes between day and night.

Saifi et al. (2012) conducted an experimental investigation of airflow in solar chimneys with a numerical simulation. The experiment was conducted with chimney slopes of 30° and 45°, and the distance between the absorber and the glass panel was set at 10 cm, 20 cm, and 30 cm. The study showed that the slope angle of the chimney and channel width affected the field velocity. Also, the temperature variation between the absorber and the glass panel changed

according to incident solar radiation. The optimal thermal pulling was at an angle of 45°.

### 1.2.3. Heated Parallel Plates

Ayinde et al. (2006) worked on heated parallel plate using a Particle Image Velocimetry (PIV) system in order to find the mean velocity in a vertical path resulting from natural convection. The researchers found that the Rayleigh number and aspect ratio had significant impact on the mean velocity profile.

### 1.2.4. Double Skin Façade

Arons (2000) developed an analytical model to test the efficiency of applying a Double Skin Facade system. The paper concluded that the double skin facade was more effective in reducing the energy consumption by 30% compared to the conventional facade system. It also concluded that the double skin facade lowered the U-value and solar heat gain coefficients of the static glass facade system. However, the research still has limitations and additional work needs to be done in order to have better analysis of the overall environmental effect of double skin facade.

Ardiani & Koerniawan (2017) tested the performance of Double Skin Facade (DSF) in an Indonesia campus building. Since Indonesia is a Southeast Asian country, which is hot and humid all the year, most of the buildings there are

equipped with air-conditioners. In order to achieve indoor thermal comfort, the authors conducted the study on the performance of double skin facade materials and concluded that perforated metal double skin facade consumed between 5% to 23% more energy than DSF in order to cool down the building.

### 1.2.5. Thermal Processing Laboratory (TPL) at McMaster University

Two ideas were examined at the Thermal Processing Laboratory (TPL) at McMaster University to reduce the energy needs by buildings: the first was the Solar Airflow Windows (SAW), Friedrich (2011), the second was the Thermal Buffer Zone (TBZ), Jan et al. (2014). The Solar Airflow Windows (SAW) is a passive air heating method that provide heating and fresh air to the building. It consists of two vertical plates where the exterior plate is made of glass. The solar radiation will hit and heat up the interior wall which will heat the air in the channel by convection. The air will rise due to the buoyancy effect then admit into the HVAC system (Heating, Ventilation, and Air Conditioning) for fresh air supply or exit to the atmosphere depend on the SAW mode that as shown in Figure 1-1. Results showed that SAW achieved up to 6% of required flow rate.

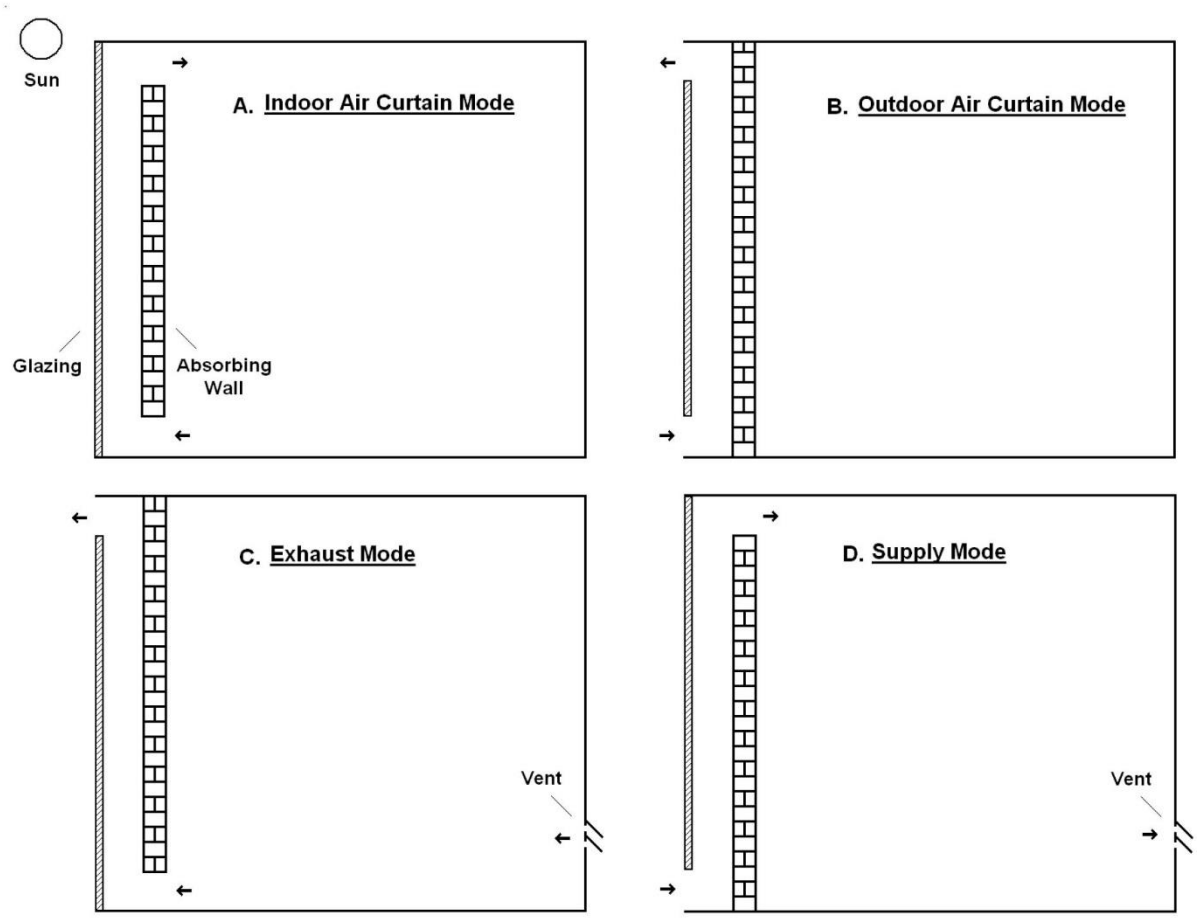


**Figure 1-1:** Solar Airflow Windows Modes. Friedrich (2011)

Although SAW showed some advantages of using passive air heating, there were some disadvantages to this method such as the loss of natural lighting in the building due to the blocking of sunlight by the interior wall. Moreover, the system performance would be sensitive to the wind speed and the building internal pressure provided by the HVAC system that could push the warm air from the cavity to the outside of the building.

Passive solar heating system, solar chimneys, Solar Airflow Windows (SAW), and Solar Dynamic Buffer Zone (SDBZ) all use open systems, which may have contributed to their disadvantages. Furthermore, they do not allow sunlight into the building, losing the advantage of natural daylight.

With these finding in mind, a new idea, the Thermal Buffer Zone (TBZ), Jan et al. (2014), was proposed to achieve the purpose of passively heating the building. A TBZ is a closed passage built around a building that allows air to passively re-distribute heat energy from solar radiation received on the south side throughout the building. The main difference between TBZ and SAW is that TBZ is a closed system which was recommended by building engineers at Halcrow Yolles, Jan et al. (2014). Also, it allows daylight to enter the building giving it the advantage of natural lighting. Thermal Buffer Zone is also known as a passive solar heating mechanism working through the principles of natural convection, stack effects, shading, and natural day lighting to optimize the use of energy sources inside the building. TBZ showed promising results on a lab scale model as a building insulation method to reduce the building energy requirements by cooling and heating. Because the Thermal Buffer Zone is a relatively new research area, there is not a lot of research about it. This research aims to develop an analytical model that can assess the effectiveness of Thermal Buffer Zone in real buildings.

## 1.3 Solar Thermal Buffer Zone

Because of the angle of the sun to the Earth during winter seasons, the southside of any building usually receives more solar energy than the north side. This unbalance in the amount of solar energy received creates an uneven heat load requirement between the south and north sides of the building. Sometimes, such unbalance causes the need for cooling and heating on the south and north sides, respectively. The idea behind the TBZ is to equalize the energy distribution around the building to reduce the temperature difference between the south and north sides of the building which would reduce the cooling load and heating load requirement of the south and north sides, respectively. The TBZ mechanism depends on the density difference between the air columns on the south and north sides. The south side of the TBZ cavity consists of two parallel glass panels which allow solar radiation to enter the cavity. This causes an increase in air temperature which reduces the air density in the southside. Due to the decreased air density, the air column in the south side becomes lighter than the air column in the north side. The difference in weight creates a driving pressure that forces the hot air to move from the south side to the north side (colder side) through the top channel. Simultaneously, the colder air is driven to move to the south side through the bottom channel as shown in Figure 1-2. Moreover, TBZ could reduce the heat loss during the night because the thermal energy stored in air inside the cavity during the day causes less energy to leave the building to the ambient which would help to keep the building warm. The TBZ will reduce the energy needs of the HVAC

system which in turn would reduce the demand for non-renewable energy such as electricity and natural gas.

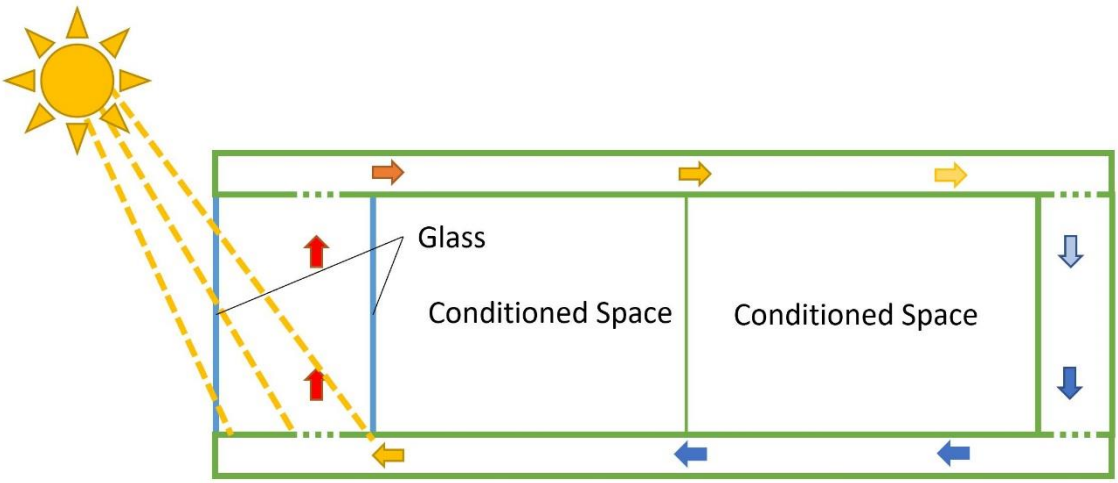


**Figure 1-2:** Solar Thermal Buffer Zone Mechanism.

## 1.4 Buoyancy Effects

The experiment is based on the application of buoyancy effects in real life. Buoyancy effect is the phenomena in which the fluid that has lighter density will move from a lower position to a higher one while the same fluid with heavier density move from a higher position to a lower one. The following formula calculates the hydrostatic force acting on a fluid:

$$P = \rho RT \qquad (1\text{-}1)$$

For solar thermosiphons, the difference between the hydrostatic force developed in the cavity and the hydrostatic force developed outside the cavity

equals the driving force of the system. Since gravity can be assumed to be constant, by changing the density of the fluid or the height of the cavity, we can change the driving pressure in a solar thermosiphon. Moreover, at the same pressure, fluid density decreases when temperature increases. Hence, when the temperature inside the solar thermosiphon cavity is increased, the driving pressure will increase.

Similarly, as the air in south side of the TBZ heats up, the driving pressure between the south and north sides increases.

## 1.5 Pressure Drop Effect

Pressure drop is calculated by comparing the pressure values of two points in a fluid-carrying network. When fluid flows in the cavity, frictional forces always exist to resist the flow, creating a pressure drop effect. Fluid kinematic viscosity and fluid velocity play the most important role in determining flow resistance. When the frictional shear force is increased, the pressure drop will also increase. However, in the TBZ, the pressure drop caused by shearing force, known as major losses, is relatively small because the air velocity in the cavity is also small. The pressure drop is caused largely by the changing direction of the flow, tube convergence, divergence, turns, and other physical properties, known as minor losses. When we increase the cross-sectional areas in the cavity, the average velocity of the air flowing in the cavity will go down, leading to decreasing pressure drop.

## 1.6 Radiation Heat Transfer

Solar radiation is the energy emitted by the sun, specifically electromagnetic energy. It contains multiple types of electromagnetic spectrums such as visible light spectrum and ultraviolet spectrum. When the solar radiation hits the glass of the building, not all of it is absorbed. The surface's transmittance, reflection, or absorption of the radiation will be determined by the material properties, incident angle of the radiation, and electromagnetic wavelength. Some of that solar radiation does not benefit the TBZ system because it is reflected by the exterior glass. Part of the solar radiation energy that is not reflected is absorbed by the exterior glass and heats the air inside the TBZ cavity via heat convection. Some of this absorbed energy will be lost to the ambient. The remaining solar radiation that was neither absorbed nor reflected, is transmitted through the glass and travels the width of the cavity before hitting the surface of the interior glass. Again, the solar radiation is split into three parts that are not necessarily of equal amount, as that is determined by the optical properties of the glass. The first part is transmitted to the inside of the building. The second part is absorbed by the interior glass making it a heat source for the air in the TBZ cavity and the inside of the building by heat convection. The third part of the solar radiation is reflected by the interior glass and bounces back to the exterior glass. The same process will repeat between the two glass surfaces, diminishing the amount of solar radiation being reflected until it is negligible. Because of this back and forth reflection, calculating the conversion

from transmitted solar radiation to thermal energy becomes complicated. Thankfully, Duffie & Beckman (1974) developed a helpful model which will be discussed in the next section.

## 1.7 Optical Properties

Duffie & Beckman (1974) model calculates the total system transmission and absorption coefficients. The total system transmission multiplied by absorption coefficients equals the optical efficiency. Then, the product of optical efficiency and the incident solar radiation on the outside of the glass will make up the total solar radiation converted to warm air at the interior glass. Different glass optical properties will have different system coefficients. In order to maximize the optical efficiency and heat gain in the TBZ, the exterior glass panel should have low reflectivity, high transmittance, low volumetric absorption, and high surface absorptivity. The interior glass panel should also have low reflectivity, but medium to low transmittance. It must also have low volumetric absorption, and high surface absorptivity.

The solar heat gain through a window system is also affected by the angle of incidence, because it affects the optical properties of the glass. The reflectivity and transmittance values do not change much when the angle of incidence is within 50° from the perpendicular, but they start to change significantly once the value of the angle goes beyond 50° from the perpendicular, making the surface completely

reflective when it reaches 90°. The incident angle in winter is often smaller than 50°, while in the summer it can be greater than 50°, thereby reflecting more of the radiation off the system.

Heat transfer also happens within the system through convection, conduction and volumetric heating. If the inside surface of the glazing system is warmer than the air going past it, it will transfer heat and contribute to the output energy. The lower the temperature of the outside air, the more heat inside the cavity will be conducted to the outside. If the temperature outside is low enough, energy absorbed in the glass surface will be conducted to the outside surroundings, lowering the temperature inside the cavity. However, since the heating system works and generate heat to the glass, not all energy absorbed in the glass is lost. The heat transfer process reduces the temperature difference between inside and outside the cavity.

## 1.8 Chimney effect

Chimney effect is also known as stack effect. Stack effect results from buoyancy forces, in which air inflows and outflows into and out of buildings, chimneys, or flue gas stacks. The higher the temperature and the taller the building, the greater the buoyancy force and stack effect. Any building is not totally sealed, there are always some holes, cracks, penetrations, or entrances that let air flow out and in, which is called air infiltration. In the winter, when the inside of the

building is warmer than the outside, the heat makes the air inside building float and escape at the top of the building. Meanwhile, the pressure at the bottom of the building decreases and makes cold air outside flow into the building. The reverse happens in the summer, when the building is cooler inside. However, the chimney effect in the summer is often weaker because the temperature difference between the inside and the outside of the building is normally not significant.

The building structure and design play an important role in changing the stack effect. For higher building with well-sealed envelope, the pressure caused by the chimney effect can be considerable. Staircases and elevators can strengthen the chimney effect while floors and fire separations can weaken the effect.

Similarly, when the air heats up in the TBZ in the south side, it rises and creates low pressure in the bottom of the south side. As a result, the colder air from the north side will be drawn to the south side from the bottom channel.

## 1.9 Objectives of Present Research

After reviewing the relevant literature on passive air heating, the following objectives were identified for the present work:

1- Develop an analytical model to calculate the effectiveness of TBZ.

2- Conduct experiments to validate the analytical model.

3- Use the analytical model to predict the effectiveness in a real building.

4- Study the effect of insulation thickness, fan, and air gap size on the effectiveness of TBZ in a real building.

# Chapter 2

# 2. Experimental Work

## 2.1 Experiment Setup

In order to have a more realistic approach for the study, an experimental setup of TBZ implemented in a scaled down floor in a building was designed and constructed. The arrangements of the solar buffer zone and radiation were similar to the setup of previous studies such as Solar Airflow Windows, Friedrich (2011) and Solar Thermal Buffer Zone, Jan et al. (2014). The distance between the heat source and the cavity channel was also adjustable, since varying radiation intensity could be applied to demonstrate the changing temperature throughout the day. Considering a south facing window in Ottawa, Canada in January on a perfectly clear day, the radiation intensity was set approximately $370\ W/m^2$, representing the daytime average. This value was based on the findings of Duffie & Beckman (1974).

### 2.1.1. Structural Frame

The setup consisted of a wooden structure with a $1\ m^3$ chamber in the middle. The chamber was encased in closed channels from four sides (south, top, north

and bottom), as shown in Figure 2-1, while the east and west sides of the chamber were open to the ambient.

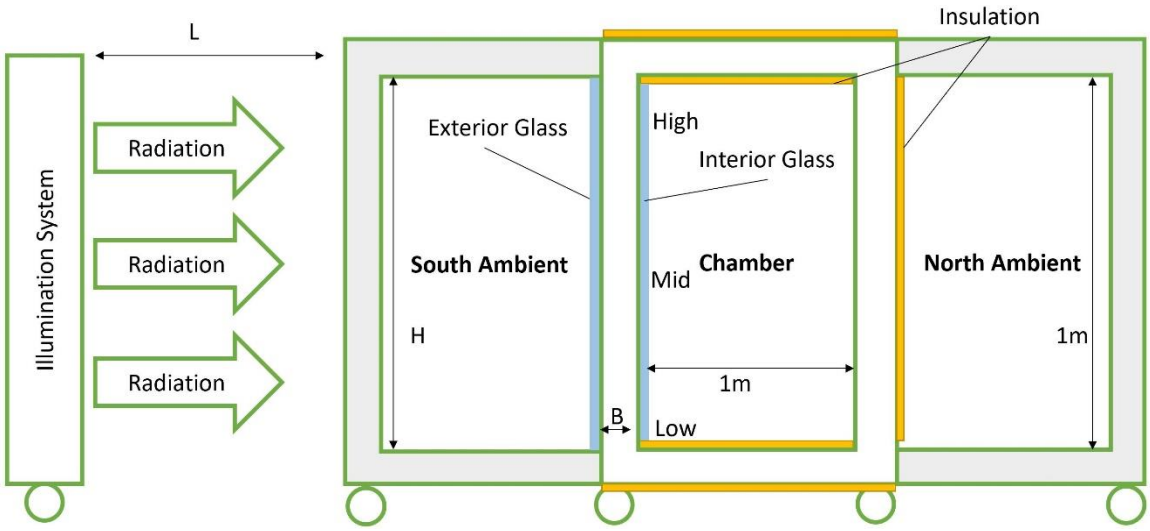


**Figure 2-1:** The Experimental Setup

The channels were made of insulation material except for the south side where glass was used to allow light and heat from the heat source to be absorbed by both the glass panels and the air in the channel. Also, cardboard was used for the inner wall of the north side TBZ where the heat was going to be transferred to the north side of the TBZ to warm chamber up and reduce the heat load. The insulation material used was an Expanded Polystyrene board, R-7.75, 38 mm thick. The south channel gap was 0.3 m wide while all other gaps were 0.1 m wide as shown in Figure 2-2. This gap size between the exterior and interior glass surfaces was judged to be the optimum gap size based on previous research Jan et al. (2014). A solar radiation source was used to provide the system with the required heat flux.

The exterior glass casing was clear and thick with a low solar absorbance while the inner glass was grey solar-shield with a high solar absorbance.

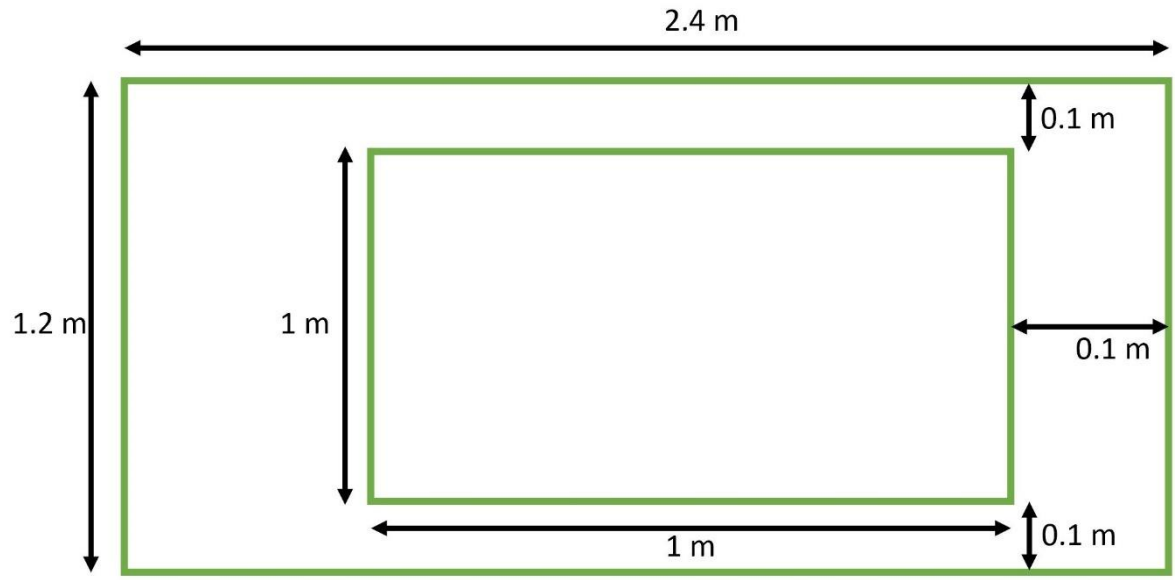


**Figure 2-2:** General Dimension of the TBZ.

### 2.1.2. Frame and Enclosure

The south side was set up with two vertical glass panels in order to examine the ideal gap width on one side of the structure. A softwood frame supported the glass and walls and held together the whole structure. The whole experiment setup was equipped with wheels so that it could be moved around the laboratory. The chamber temperature, taken at the three-dimensional center of the chamber, was similar to that of the ambient (the lab) due to the completely open east and west sides of the chamber.

The frame consisted of plywood, transparent acrylic glass, Expanded Polystyrene boards and corrugated sheet plastic. The base of the frame was made of plywood so that it could support the weight of the model. One side of the frame was made of transparent acrylic glass, to ensure visibility of the velocity probe. Since corrugated plastic sheets and Expanded Polystyrene boards were low-cost, flexible, and lightweight, they were ideal materials to be used with plywood and acrylic glass. Since plywood was hard and acrylic glass and plastic sheets were pliable, they could be easily fit into position with the use of silicon, foam and tape. The exterior glass used was standard clear window glass and was mounted on a lightweight aluminum frame structure.

### 2.1.3. Glass Properties

As discussed earlier, different optical properties have different optical efficiencies. In this experiment, a standard 6 mm thick window-panes were used. The south side was equipped with two window-panes while the north side was fitted with corrugated plastic sheets. The exterior glass panel in the south side was standard clear window glass, which had a high solar heat gain coefficient of 0.83, meaning 83% of the solar radiation energy was transmitted through the glass to the TBZ. Conversely, the interior glass pane, which was Solarshield Grey glass, was less transmittable and had a lower solar heat gain coefficient of 0.54. The energy that was not transferred through the interior glass would be transferred to the air in the TBZ cavity. Moreover, as ultraviolet light contains more energy and

shorter wavelengths than visible light, it may contribute to heating the glass more than the visible light. The exterior glass had an ultraviolet light transmittance value of 0.54 and the interior glass had an ultraviolet light transmittance value of 0.25. The velocity probe was inserted in the holes through the interior glass.

### 2.1.4. Illumination System

The sun's radiation has a uniform intensity across all wavelengths of its radiation. Acquiring a radiation source with the sun's surface temperature (5777 °K) and spectrum would prove extremely difficult. Therefore, a more reasonable and cost-effective alternative was to reuse the illumination system constructed for SAW research, Friedrich (2011). The system came with Quartz Tungsten Halogen (QTH) light bulbs which had blackbody spectral properties of 3000 °K to 3300 °K and an average radiation intensity of 1000 $W/m^2$.

Figure 2-3 illustrates how the illumination system provided less intensity in the visible spectrum than the sun, because the black body had the temperature of 3200 °K. However, the majority of the energy coming from the QTH light bulbs were in shorter wavelengths. The glass was opaque to long wavelength radiation and more transmittable to short wavelength radiation. Therefore, the black body would give thermal results that were close to those of the sun's radiation.

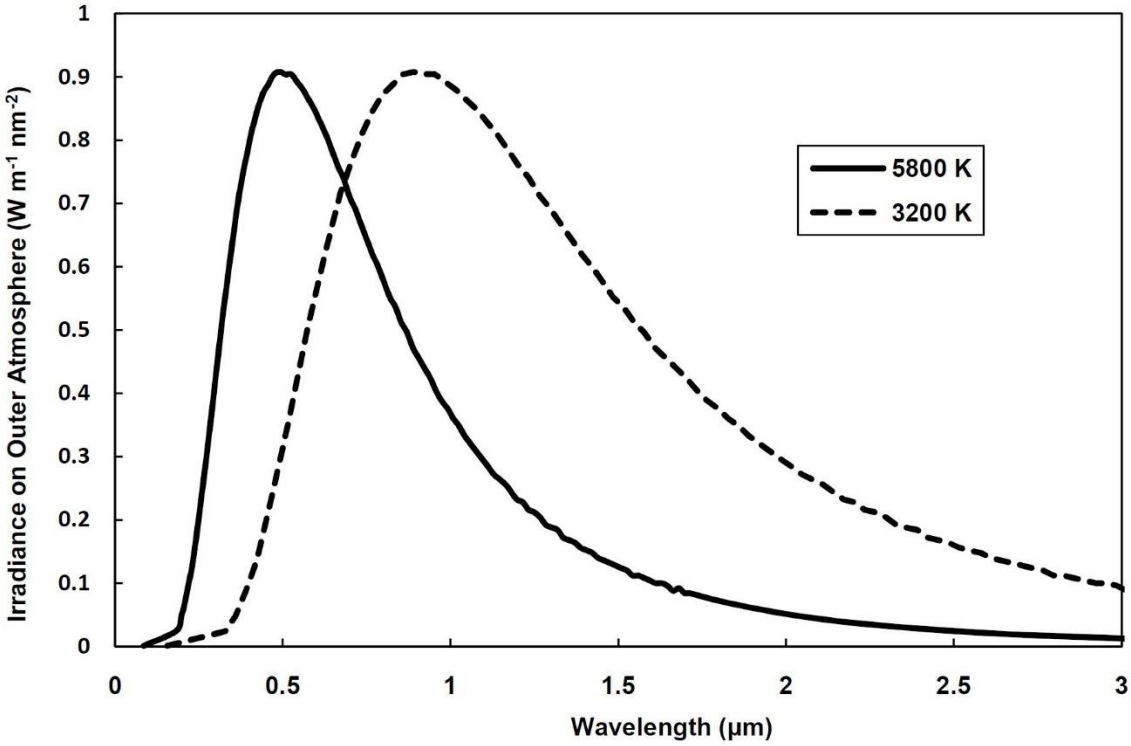


**Figure 2- 3:** Spectral Distribution of Solar and Black Body Temperature of 3200°K. Friedrich (2011).

The non-uniform heating pattern seen in Figure 2-4 was produced by the light diverging from the four QTH light bulbs. The points in the glass surface which were located directly in front of the light bulbs received more energy than the glass corners. Although the intensity dwindled with radial distance from these points, the heat flux at the center of the glass surface was higher due to the overlapping of the intensities spreading from them. This behavior created a non-uniform heat flux which may have affected the uniformity of the mass flow rate.

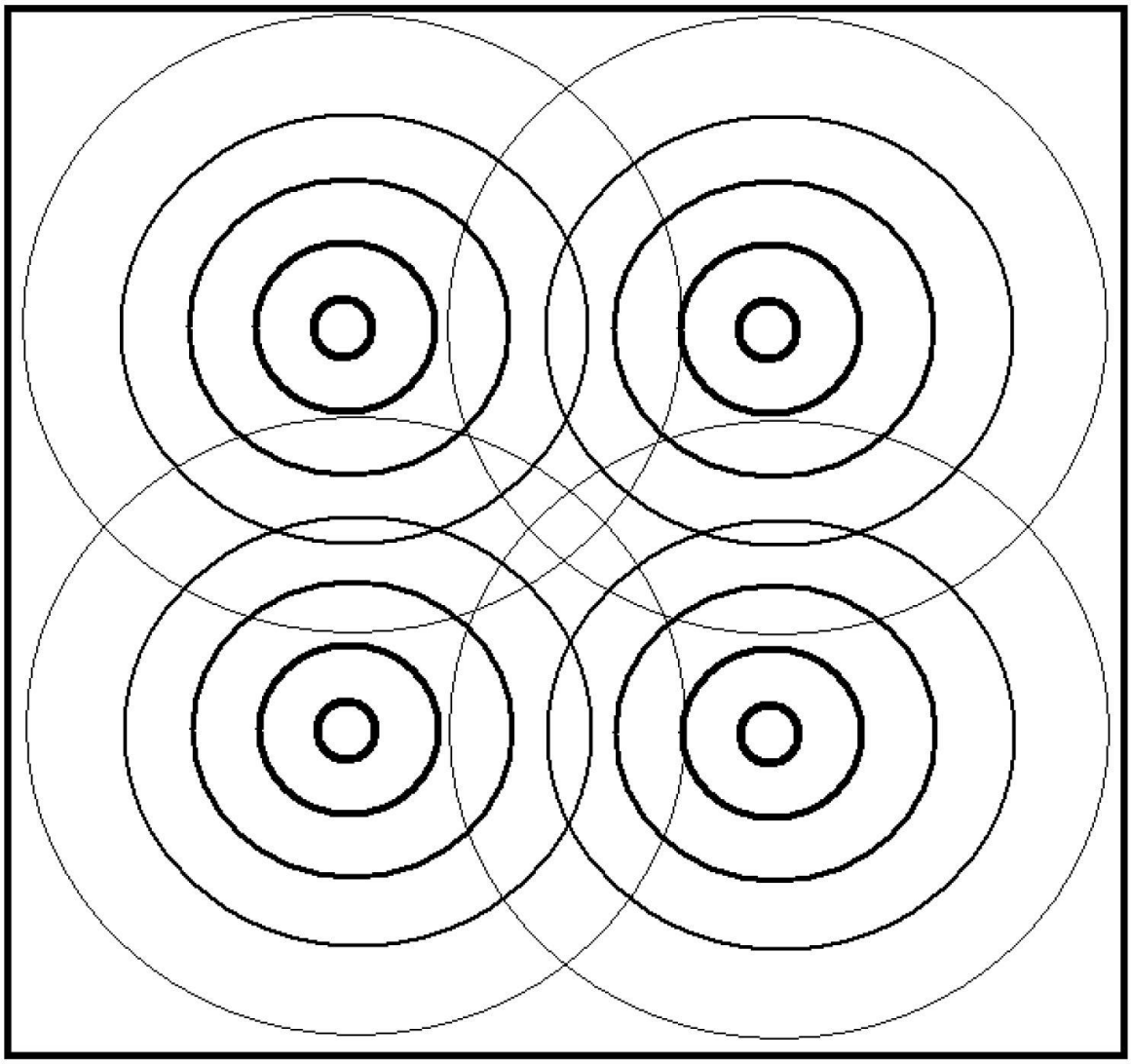

**Figure 2-4:** Overlapping heat flux intensities on the illuminated surface from the heat source. Friedrich (2011).

### 2.1.5. Pyranometer

The intensity was measured using a Hukseflux LP02 solar pyranometer with an accurate operation range of 305-2800 nm which covers most of the solar

spectrum energy. To detect the heat flux intensity in the south side, a square grid was placed 9 cm away from where the intensity was to be measured.

### 2.1.6. Data Acquisition System

A Hydra Data Logger Series II records the voltage readings of the pyranometer, thermocouple, and velocity probe. Twenty-channel interchangeable input cards were used to switch between the components. The experiment was conducted in steady state in order to be able to assume that temperatures and velocities would be constant when they were measured at different periods. That assumption was necessary as it was not feasible to measure all the thirty-eight thermocouples instantaneously.

### 2.1.7. Temperature Measurements

Figure 2-5 shows where the surface and air temperature measurements were taken in the thermal buffer zone. Centerline temperature profiles were taken on the vertical surfaces to ensure that the values were comparable to the analytical model.

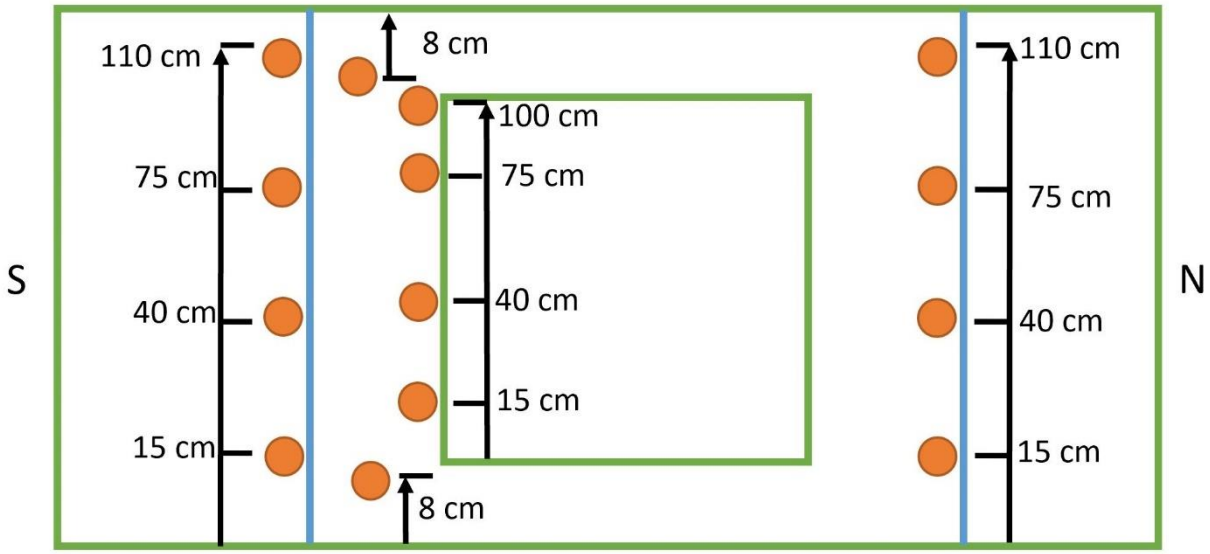


**Figure 2-5:** Thermocouples Locations for Temperature Measurement

Type T thermocouples (junction diameter: 2 mm) served as means to measure the temperature. They were taped to the surfaces and covered in tin foil to reduce the influence of heat flux from the illumination system. Two thermocouples were placed in the inlet and outlet of the south side to measure air temperature. The hot-wire probe would measure the air temperature at different elevations between the inlet and outlet locations in the south side in addition to the middle of the north side. To reduce the effect of direct radiation in the south side, shading was provided to the hot-wire probe during measurement-taking. All other remaining thermocouples were used to measure the temperatures of the different surfaces.

The chamber temperature changed throughout the duration of experiment, particularly near the walls where the temperature varied up to 3 ℃ within a couple of hours of heat flux exposure. Temperature profile accuracy could be affected by factors such as thermocouple probe sealing and illumination system radiation.

### 2.1.8. Velocity Measurements

The velocity probe was inserted to a maximum of 15 cm into the cavity. The omnidirectional ComfortSense probe was used to take the velocity measurements in the four locations in the centerline as seen labelled in Figure 2-6. The ComfortSense probe detects velocity by detecting the voltage which converts to velocity via Microsoft Office Excel spread sheet that provided from the suppler, Appendix A showed the details of the conversion. The ComfortSense probe could detect very low velocities but suffered some limitations such as not capturing turbulent properties and high velocity gradients close to the wall. The ComfortSense was factory-calibrated to near-zero velocities and also had a hot-wire sensors that could measure the temperature.

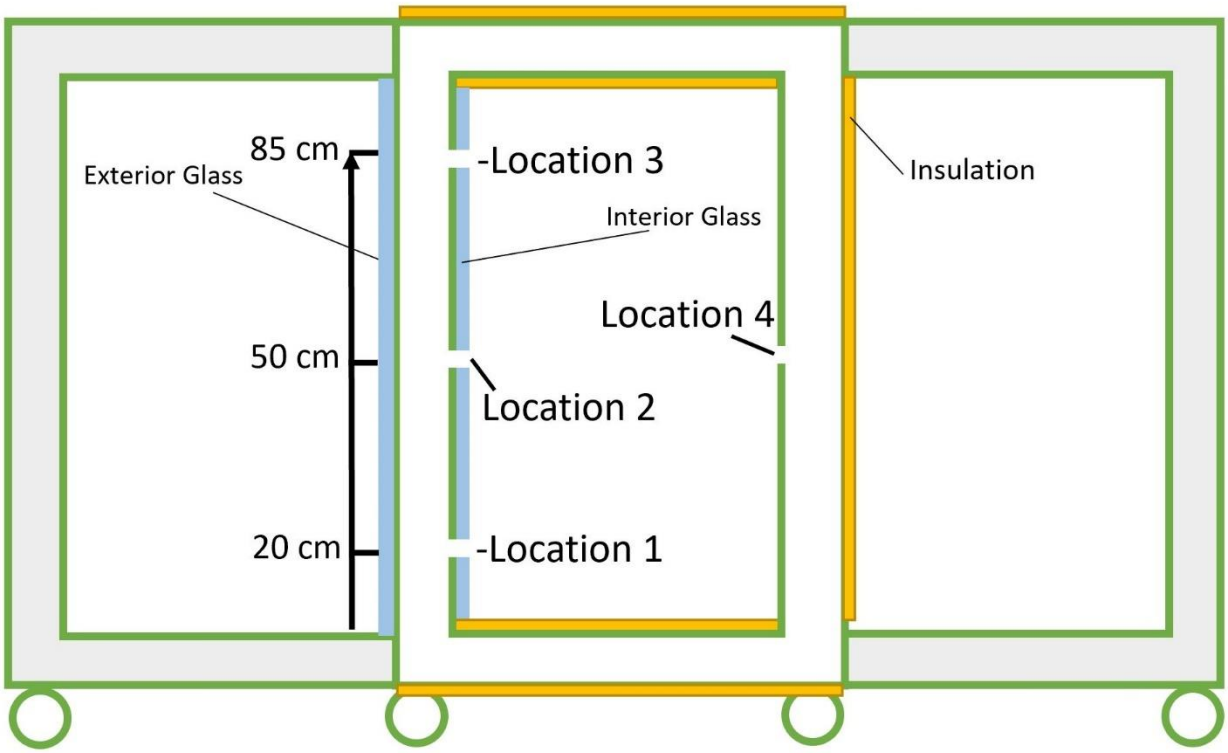


**Figure 2-6:** Velocity and Temperature Measurement Locations.

The velocity value represents the time-averaged mean velocity in each location, which was taken in order to minimize the effect of the turbulent flow. One hundred samples were taken at each location as done by Ryan & Burek (2010), Friedrich (2011) and Jan et al. (2014). The readings were taken at one second intervals and averaged per two minutes. There is a difference of around 10% between the means of the first and second one hundred samples, indicating an increase in velocity variability.

Location 1, 20 cm above the bottom of the experimental setup, had the lowest mass flow rate. This is explained through the findings in the work of La Pica et al. (1993) where recirculation in the lowest portion was captured by means of smoke.

Near zero velocities were not measured accurately with a hot-wire velocity probe due to the natural convection flow caused by the heated-up probe. Measurement uncertainty increases when velocity is below 0.05 m/s, which was the case in many of the measurement taken. The lowest point in the manufacturer's calibration curve is 0.05 m/s, meaning any values below that point have a higher uncertainty. By shifting the manufacturer's calibration curve down so that its lowest point sits at 0.0027 m/s (lowest point in the calibration data of the velocity probe) instead of 0.05 m/s, these small values were corrected and any velocity below that value was considered zero.

### 2.1.9. Calibration

#### 2.1.9.1. Pyranometer

The pyranometer calibration of 14.8 μV per $W/m^2$, with a validity range of (0-2000) $W/m^2$, was set by the manufacturer.

#### 2.1.9.2. ComfortSense Probe

Calibrated by the manufacturer, the ComfortSense probe came with a calibration curve connecting the velocity and temperature in a nonlinear relationship.

#### 2.1.9.3. Thermocouples

Thermocouples were used to measure the surface temperature of the exterior and interior glass surfaces as well as the exterior north side wall. Also, the temperatures of the inlet and outlet of the south side cavity were captured using the thermocouples.

The thermocouples were calibrated using the freezing and boiling temperatures, and the built-in calibration curve in the Hydra Series II was used. The south side had a higher number of thermocouples to accommodate the wider range of temperature values, unlike the north side.

### 2.1.10. Uncertainty Analysis

Two sources of independent uncertainty were taken into consideration: the first was the equipment uncertainty in measurement as provided by the manufacturers, the second was the experiment's uncertainty. Propagating the uncertainties through the relevant equations results in the dependent variable uncertainty. The propagation of uncertainty equation (2-1) is as follows, Figliola & Beasley (2000):

$$u_R = \pm\sqrt{\sum_{i=1}^{L}\left(\frac{\partial R}{\partial x_i}u_{x_i}\right)^2} \qquad (2\text{-}1)$$

Where: R= Result; $u_R$=uncertainty in R, L=Number of independent variables (x)

The uncertainty values propagated are:

- Velocity uncertainty = ±0.02 m/s
- Air temperature uncertainty = ±1.0 ℃
- Spatial distance uncertainty = ±0.0001 m
- Pyranometer uncertainty = ±10%

The mass flow rate is depending on three variables which are density, velocity and cross-section areas seen in equation (2-2). In order to measure the uncertainty of the mass flow rate $(u_{\dot{m}})$, the uncertainty of density, velocity and cross-section area must be known. The uncertainty of the velocity and cross-section area is known but the uncertainty of density should be calculated.

$$\dot{m} = \rho v A \qquad (2\text{-}2)$$

Base on equation (2-3) the density uncertainty $(u_\rho)$ is depending on two variables which are pressure and temperature.

$$\rho = \frac{P}{RT} \qquad (2\text{-}3)$$

After taking the partial derivative with respect to pressure and temperature, the uncertainty of density is calculated in equation (2-4)

$$u_\rho = \pm\sqrt{\left(\frac{\partial \rho}{\partial P} u_P\right)^2 + \left(\frac{\partial \rho}{\partial T} u_T\right)^2} \qquad (2\text{-}4)$$

Now, we can calculate the partial derivative of mass flow rate with respect to density, velocity and cross-section area. the uncertainty of mass flow rate is calculated in equation (2-5)

$$u_{\dot{m}} = \pm\sqrt{\left(\frac{\partial \dot{m}}{\partial \rho} u_\rho\right)^2 + \left(\frac{\partial \dot{m}}{\partial v} u_v\right)^2 + \left(\frac{\partial \dot{m}}{\partial A} u_A\right)^2} \quad (2\text{-}5)$$

For the current work, the expected uncertainty would be $\pm 10.7\%$ Jan et al. (2014) as the current used instruments are same as the instruments used in the previous project.

## 2.2 Experimental Results

Two experiments were conducted. The only difference between the two experiments were the ambient and chamber temperatures. The ambient and chamber temperature in the first experiment were both 27 ℃ and in the second experiment were 24.35 ℃.

The first stage of the experiment is to make sure that the experimental setup is exposed to the optimum amount of heat flux, which is equivalent to the average heat flux during the daylight hours in January in Ottawa. This amount of energy will be treated as the total incident energy arriving to the exterior glass in the south side. A pyranometer was placed in front of the exterior glass to take

measurement of the heat flux. After adjusting the distance between the heat source and the exterior glass to 1.38 m, the average heat flux was measured to be around 370 $W/m^2$. Moreover, the pyranometer was placed inside the chamber facing the interior glass to measure the amount of heat flux entering the chamber. Table 2-1 shows the average heat flux values.

**Table 2-1:** Amount of Heat Flux Received.

| Type of Measurement | Distance from illumination (m) | Heat Flux (W/m^2) | |
|---|---|---|---|
| | | Experiment-1 | Experiment-2 |
| Heat Flux in front of Exterior Glass | 1.38 | 369.8 | 370.5 |
| Heat Flux Behind Interior Glass | 1.70 | 65.5 | 75.2 |

It is worth mentioning that the average heat flux that enters the chamber is much lower than the total incident heat flux. There two reasons for this sudden decrease: the first is the effect of the distance between the illumination system and the interior glass which can be seen in Appendix B, the second is absorptivity of the interior glass. Due to the high absorptivity of the interior glass, it is highly expected that most of the heat flux will remain in the TBZ system once it has entered it.

The experimental setup was exposed to the heat source for 4 to 5 hours before any measurements were taken to ensure the system has reached steady state. Moreover, in order to confirm that the system was stable and in steady state, more than 500 velocity and temperature readings were taken with the hot-wire velocity

probe for each hole at a rate of approximately one reading per second, making the duration of the first measurement more than 10 minutes. Beyond confirming the steady state, the large number of readings taken during the first measurement for each hole was necessary to eliminate the effect of the ambient air that entered from the hole during hot-wire velocity probe insertion. During the first measurement, the mean temperature values of the first and second 100 readings differed by 5%, while the means of the fourth and fifth 100 readings differed by under 2%. All other measurements in each hole were taken at 3.5 minutes interval at the same rate of nearly one reading per second, and gave more than 200 readings. The means of first and second 100 temperature readings in each hole differed by less than 2%. The arrows shown in Figure 2-7 represent the air movement direction inside the TBZ cavity.

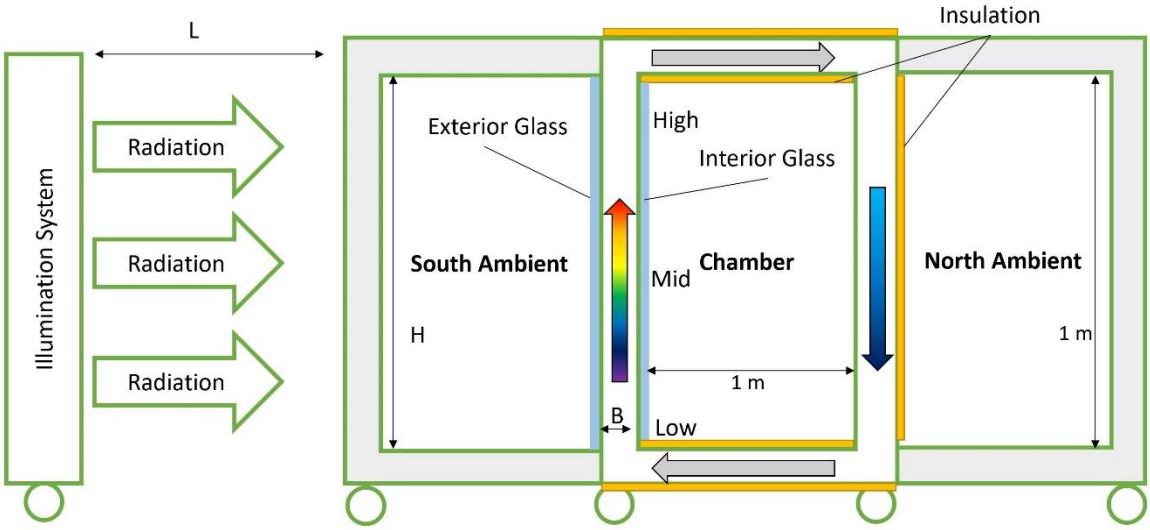


**Figure 2-7:** Movement of the Air Inside the Cavity.

After confirming that the system reached steady state, the exterior and interior glass surface temperatures were recorded. The glass surface temperatures were continuously stable and steady during experiments conducted. The results of both experiments were almost identical. Table 2-2 and 2-3 shows the surface temperature of the exterior and interior glass respectively.

**Table 2-2:** Temperature of Exterior Glass.

| South Exterior Wall Surface Temperature | | | |
|---|---|---|---|
| Hight (cm) | Left (°C) | Center (°C) | Right (°C) |
| 110 | 39.6 | 39.4 | 38.4 |
| 75 | 40.3 | 38.4 | 37.5 |
| 40 | 41.3 | 38.5 | 38.6 |
| 15 | 41.6 | 39.0 | 40.0 |

**Table 2-3:** Temperature of Interior Glass.

| South Interior Wall Surface Temperature | | | |
|---|---|---|---|
| Hight (cm) | Left (°C) | Center (°C) | Right (°C) |
| 100 | 40.8 | 42.1 | 40.5 |
| 75 | 41.5 | 42.4 | 41.1 |
| 40 | 40.5 | 41.7 | 40.2 |
| 15 | 40.5 | 41.8 | 40.1 |

The surface temperature values of the exterior north wall in Table 2-4 indicate that the hot air warms up the surface of the north wall when it arrives there, thereby achieving one of the main goals of TBZ.

**Table 2-4:** Temperature of Exterior North Wall.

| North Exterior Wall Surface Temperature | | | |
|---|---|---|---|
| Hight (cm) | Left (°C) | Center (°C) | Right (°C) |
| 110 | 35.7 | 37.7 | 36.0 |
| 75 | 35.1 | 35.6 | 35.2 |
| 40 | 35.4 | 34.7 | 34.5 |
| 10 | 33.7 | 34.6 | 33.7 |

Due to the limitation of the hot-wire velocity probe length, the air temperature and velocity were measured in the south side from the interior glass at a depth of 15 cm in the TBZ gap, the total depth of which is 30 cm. Furthermore, the velocity profile could be assumed symmetrical because the temperatures of the exterior and interior glass plates were very close, Habib et al. (2002) and Jan et al. (2014).

Moreover, at a distance of 0 cm, the air temperature and velocity readings were represented by the surface temperature taken using thermocouples and 0 m/s velocity due to the no slip condition. Figures 2-8 through 2-15 show the velocity and air temperature profiles for four locations in both experiments.

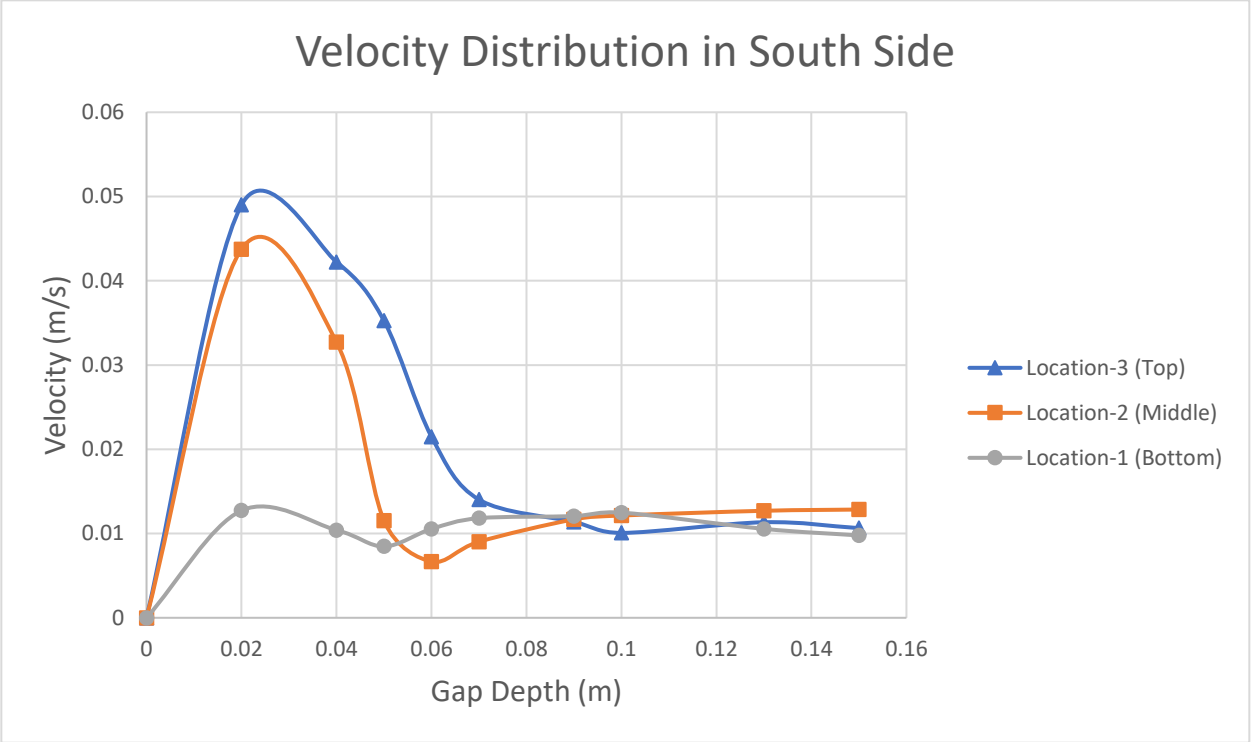


**Figure 2-8:** Velocity Distribution in South Side in Experiment-1.

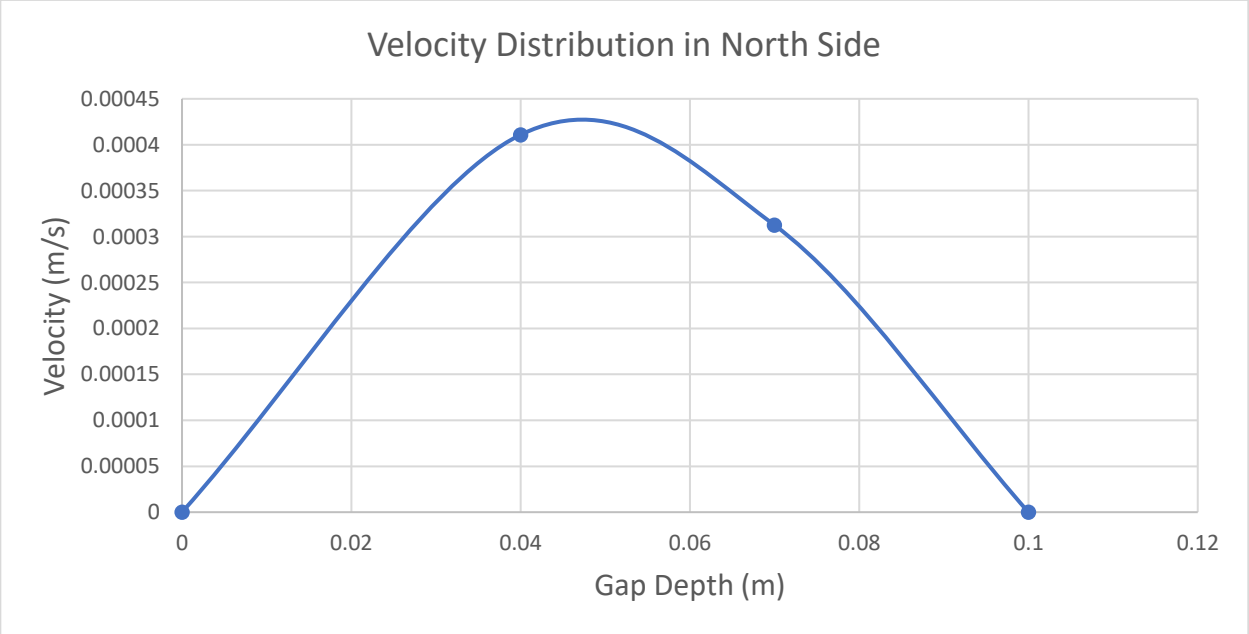


**Figure 2-9:** Velocity Distribution in North Side in Experiment-1.

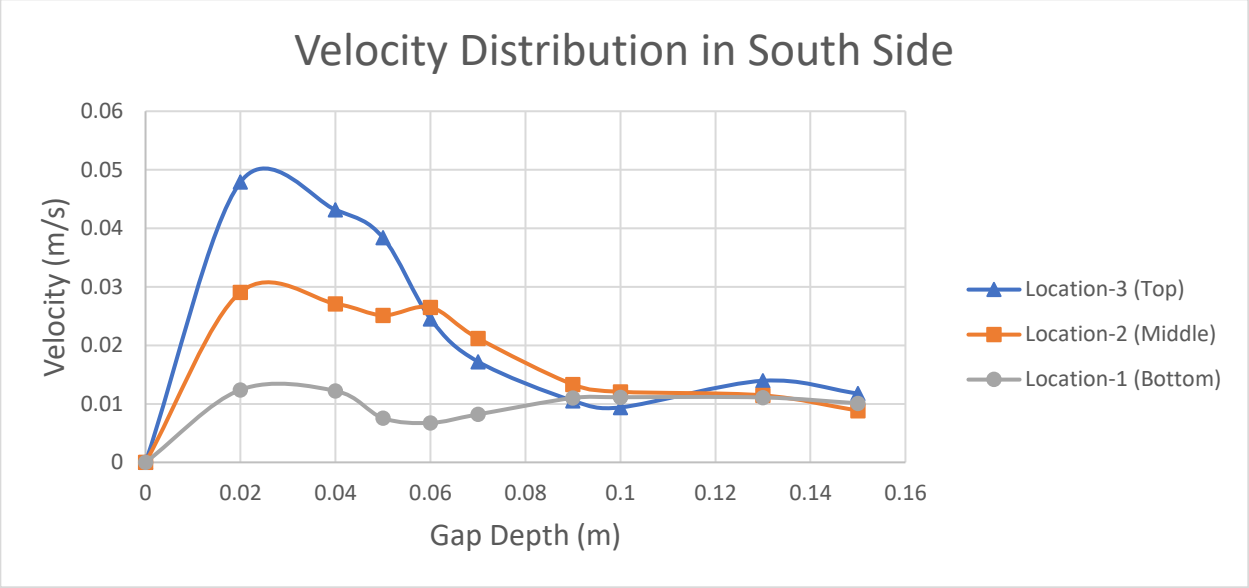


**Figure 2-10:** Velocity Distribution in South Side in Experiment-2.

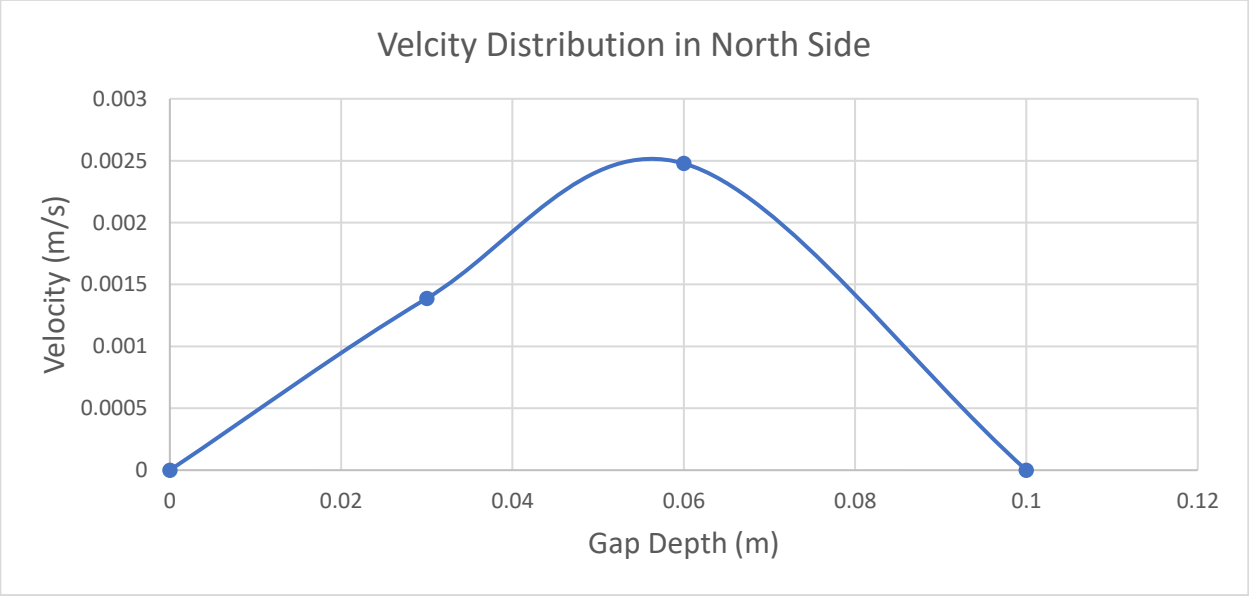


**Figure 2-11:** Velocity Distribution in North Side in Experiment-2.

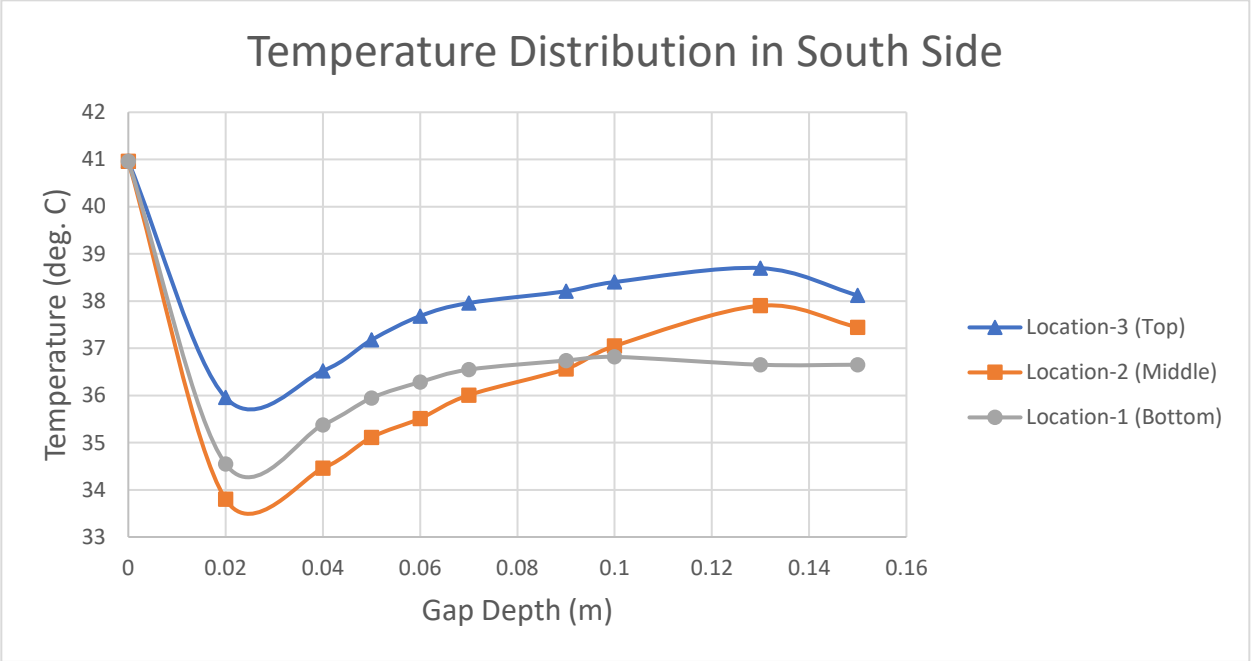


**Figure 2-12:** Temperature Distribution in South Side in Experiment-1.

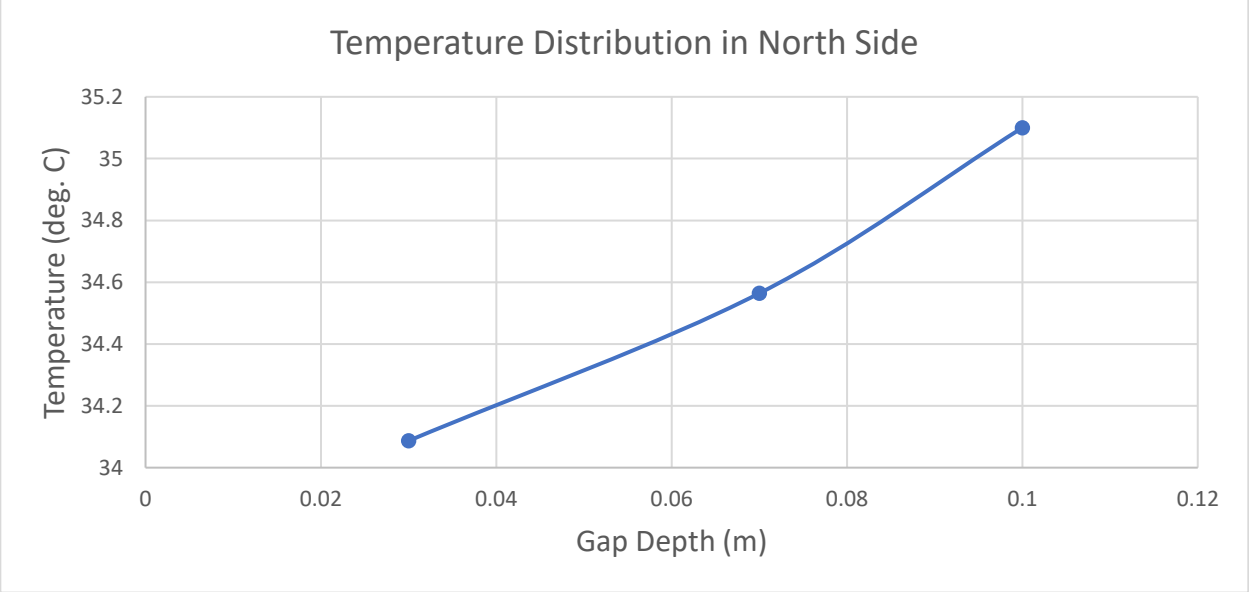


**Figure 2-13:** Temperature Distribution in North Side in Experiment-1.

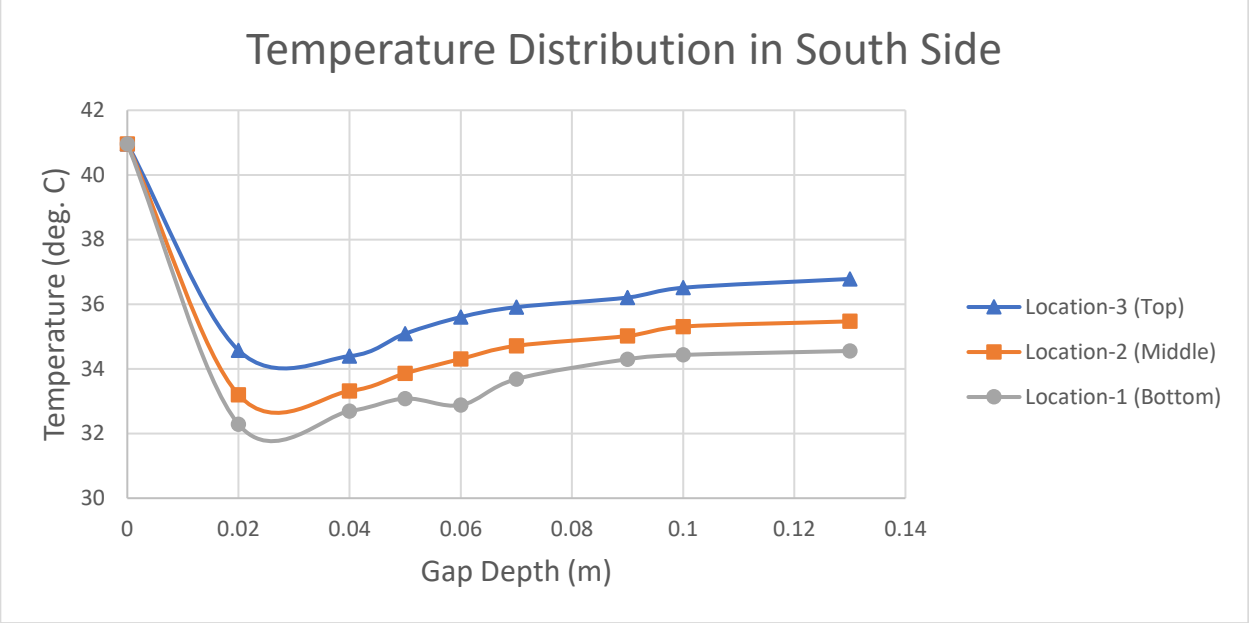


**Figure 2-14:** Temperature Distribution in South Side in Experiment-2.

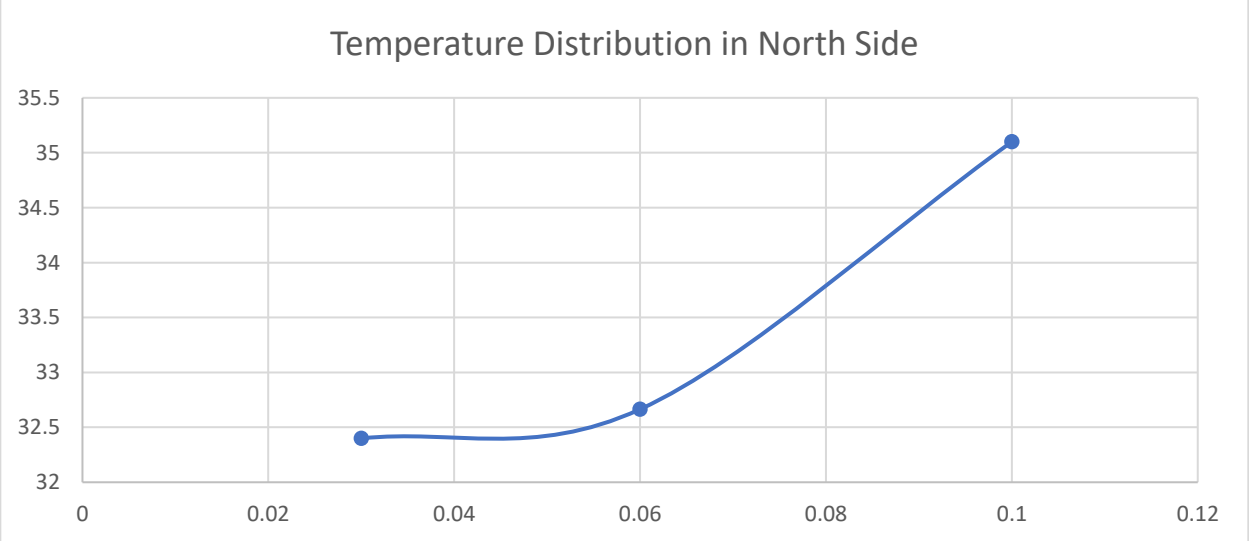


**Figure 2-15:** Temperature Distribution in North Side in Experiment-2.

Figures 2-8 and 2-10 show the velocity profile in the south side where the velocity is highest near the wall and starts decreasing a few centimeters away from

the wall. There is one velocity peak shown in these two figures. According to our previous assumption that the velocity profile is symmetrical based on Habib et al. (2002) and Jan et al. (2014), the air velocity will peak once more a few centimetres before the exterior glass surface. Therefore, the velocity profile of the second half of the TBZ gap is assumed to be the same as the first half. Moreover, the exterior and interior glass surfaces transferred the heat to the air cavity via natural convection, creating a buoyancy force that pushed the air up near the glass surfaces. Due to the resistance in the system and different velocities between the sides and the middle of the gap, a convection loop could have been created, thereby reducing the amount of flow reaching the north side. It was difficult to measure the recirculation due to very low velocity.

Figures 2-12 and 2-14 show the air temperature profile in the south side where the temperature is lowest near the wall and increases the closer the air is to the middle of the gap. This behaviour supports the previous analysis of the velocity profile: due to the convection loop, the temperature built up in the middle of the gap while the sides near glass walls had lower temperature because the higher local velocity brought cold air from north side. Although Experiment-1 showed higher temperature in the south side cavity than Experiment-2, the difference between the top and bottom ends of the south side cavity in both experiments is almost the same at 5.30 ℃ and 5.37 ℃ respectively. The overall higher temperatures in Experiment-1 were due to the ambient temperature. As mentioned before, the ambient temperature in experiment-1 was 27 ℃ while in experiment-2 it was 24.35

℃. Furthermore, the air temperature rises as the air goes up due to the increase in the energy absorbed by air.

Table 2-5 shows the mass flow rate that was measured in each location. There are multiple reasons for the large variation between the mass flow rate measurement in the different locations. The recirculation could be one of the main reasons for these differences. Also, the absolute value of the air velocity would be inaccurate when the flow is not perpendicular to the hot-wire probe. Moreover, the non-uniform heating of the TBZ cavity due to three-dimensional effect of illumination system and hot air leakage to the chamber and ambient from the holes during the measurements plays a role in the variation. The mass flow rate at Location-1 is the lowest in the south side due to the high recirculation La Pica et al. (1993). Also, the mass flow rate is low because the thermocouple wires placed inside the TBZ cavity pass through the bottom of the channel and go out of the cavity to measure the glass surface temperature, which disturbs the air movement and may create more recirculation. Finally, due to the aforementioned thermocouple wires exiting the cavity and the holes necessary for the hot-wire velocity probe, the experimental setup was not fully insulated. All the above factors play a role the variation in the mass flow rate inside the TBZ cavity.

**Table 2-5:** Mass Flow Rate in Each Location

| ***Type of Measurement*** | **Mass Flow Rate (kg/s)** | |
|---|---|---|
| | ***Experimental-1*** | ***Experimental-2*** |
| Location-1 | 3.64E-03 | 3.40E-03 |
| Location-2 | 5.91E-03 | 6.12E-03 |
| Location-3 | 7.32E-03 | 7.67E-03 |
| Location-4 | 2.94E-05 | 1.28E-04 |

As the air is heated by the glass surfaces, the velocity increases on the sides of the cavity which results in an increase in the mass flow rate. Location-2 and 3 showed that the velocity profile was more developed and uniform and less affected by circulation, which resulted in similar mass flow rate values. Based on these observations, the mass flow rate was calculated based on the average of location-2 and 3. Moreover, some of the hot air arrived to the north side and warmed the cavity and surface walls.

While the initial condition of the experiment could be controlled, the conditions of the lab could not. Although attempts were made to control it, the changing temperature in the lab affected the heat loss and gain in the experimental setup. Furthermore, the velocity measured at one single line which was used to calculate the mass flow rate. In future work, the conditions of the room housing the experimental setup must be controlled, and the velocity needs to be measured at several locations in order to capture the bulk velocity which could be representative of the actual mass flow rate.

# Chapter 3

# 3. Analytical Model

## 3.1 Analytical Model Development

The analytical model is developed using MATLAB to predict the effectiveness of the TBZ in a real building. The model consists of two sub-models: the flow and thermal sub-models. After the model is translated into code, the percentage of error in the results of the analytical model has been examined, and the analytical model output was validated by comparing its results with the experimental results. The model has been refined and improved accordingly to produce the most accurate prediction possible of the effectiveness of the TBZ in buildings.

**Analytical Model Development:**

The analytical model is developed to adapt to the user input and predict the effective of the TBZ in buildings of different sizes, material, location, ... etc. Below is a list of the different parameters that can influence the effectiveness of the TBZ.

- Room temperature.
- Ambient temperature.
- Building size.
- Air gap size of the TBZ.
- Glass thickness.
- Wall thickness.

- Insulation thickness (if available).
- Wall thermal conductivity.
- Insulation thermal conductivity.
- Glass thermal conductivity.
- Pressure of the fan (if applicable).
- Incident solar radiation.
- Transmittance of both exterior and interior glass of the TBZ.

Random TBZ corner temperatures were introduced to initiate the calculations. These temperature values were used to initiate the calculation of the thermal sub-model which would cause the flow sub-model to begin to generate values, and set the analytical model in motion. The analytical model also calculates the affected heat flax in the TBZ cavity based on the value of incident solar radiation and optical properties.

### 3.1.1. The Flow Sub-Model

The purpose of the flow sub-model is to find the mass flow rate in the TBZ system based on the current temperatures within the TBZ cavity. Due to the nature of the TBZ system, the density of the air decreases in the south side of the TBZ cavity due to energy absorbance from the solar irradiance. After that the density changes depending on energy gain or loss through the system. Therefore, the

density in each side of the TBZ cavity must be calculated by the ideal gas law which is based on temperature change as seen in equation (3-1).

$$P = \rho RT \tag{3-1}$$

The calculated density is used to find the force (weight) (3-2) using Newton's Second Law of Motion.

$$W = ma = \rho Vg = \frac{PVg}{RT} \tag{3-2}$$

The difference between the south and north pressures creates the driving pressure. This driving pressure must be equal the total pressure drop in the system (3-3), so all major and minor losses were calculated and combined into the total head loss (3-4,3-5 & 3-6).

$$P_{drive} = P_{drop} = \rho g h_L \tag{3-3}$$

$$h_l = f \frac{L}{D_H} \frac{v^2}{2g} \tag{3-4}$$

$$h_{lm} = K \frac{v^2}{2g} \tag{3-5}$$

$$h_L = \sum h_l + \sum h_{lm} \tag{3-6}$$

Based on the relationship between mass flow rate and velocity (3-7), all head losses are function of the mass flow rate (3-8 & 3-9).

$$\dot{m} = \rho v A \quad (3\text{-}7)$$

$$h_l = f \frac{L}{D} \frac{\dot{m}^2}{2g\rho^2 A^2} \quad (3\text{-}8)$$

$$h_{lm} = K \frac{\dot{m}^2}{2g\rho^2 A^2} \quad (3\text{-}9)$$

The friction factor will be calculated using the Reynold number (3-10, 3-11 & 3-12)

$$Re = \frac{\rho v D_H}{\mu} \quad (3\text{-}10)$$

$$f = \frac{70}{Re} \quad \text{(Laminar Flow)} \quad (3\text{-}11)$$

$$f = 0.316 Re_{D_H}^{-0.25} \quad , Re_{D_H} \leq 20{,}000 \text{ (turbulent Flow)} \quad (3\text{-}12)$$

The current mass flow rate can be found by substituting equations (3-6), (3-8) and (3-9) into equation (3-3) as seen in (3-13).

$$P_{drive} = P_{drop} = \dot{m}^2 \left[ \left( f \frac{L}{D} \frac{1}{2\rho A^2} \right) + \left( K \frac{1}{2\rho A^2} \right) \right] \quad (3\text{-}13)$$

At the end of each loop, the program compares the current mass flow rate with the initiated or the previously calculated mass flow rate to check if the system has reached convergence. The flow sub-model attempts to calculate the mass flow rate resulting from certain temperature differences by equating the driving pressure to the resistance pressure. However, in order to accomplish this, the temperatures must be known, which are determined using the thermal sub-model. The updated

mass flow rate will update the velocities, Reynold numbers and friction factors which become input to the thermal sub-model

### 3.1.2. The Thermal Sub-model

The thermal sub-model calculates the heat gained or lost within the system, and the temperatures in each side of the TBZ cavity. First, the amount of heat entering the system from the south side is calculated based on the size of the building and the glass properties. After that, the thermal sub-model considers each side in the TBZ cavity as a separate control volume and integrates the thermal resistance and the conservation of energy equations (3-14).

$$\dot{Q} = \dot{m} c_p \Delta T = \frac{T_{space} - T_{ambient}}{\sum R} \quad (3\text{-}14)$$

Three types of thermal resistance are used in the thermal sub-model and they are: thermal conduction (3-15), thermal natural convection (3-16), and thermal forced convection (3-17):

$$R_c = \frac{L}{k A_s} \quad (3\text{-}15)$$

$$R_n = \frac{1}{h_n A_s} \quad (3\text{-}16)$$

$$R_f = \frac{1}{h_f A_s} \quad (3\text{-}17)$$

The thermal forced convection used in the TBZ channel results from the pressure difference that was created between the south and north. Therefore,

Nusselt number correlations for laminar or turbulence must be used in order to determine the forced convection heat transfer coefficient (3-18 & 3-19)

$$Nu_{D_H} = \frac{h_f D_H}{k} = 7.54 \qquad \text{(Laminar Flow)} \qquad \textit{(3-18)}$$

While for turbulent flow:

$$Nu_{D_H} = ((f/8)((Re) - 1000)Pr)/(1 + (12.7(f/8)^{0.5}(Pr^{2/3} - 1)) \qquad \textit{(3-19)}$$

The thermal sub-model will calculate the heat gain or loss in each control volume either to outside or inside the building. Temperatures are calculated in each side of the TBZ cavity based on the integration of thermal resistance, conservation of energy, and the amount of the mass flow rate passing through the channel. At this point the program compares the current temperature with the previous temperature to check if the system has reached convergence and if it has not, another loop will take place where the new temperatures would be the new input in the flow sub-model.

The thermal sub-model is essentially a heat balance that equates the heat input to the heat output. A key part in the success of the thermal sub-model is the flow rate provided by the flow sub-model. The two sub-models are interconnected, each needing input values coming from the other to continue calculating. The analytical model compares the last two mass flow rates and temperatures and if the difference between any of them is more than 0.1%, then the system will initiate

another loop where the current output would be the new input until the flow and thermal sub-models both reach convergence (steady state).

Finally, the analytical model performs two additional checks for the thermal sub-model. The first one is to compare the net energy gained by the air in the south side to the total energy gain or loss in the other sides. The second one is to compare the total amount of energy that entered the system from the south side to the total energy gain or loss in all other side plus the energy loss in the south side.

### 3.1.3. Validation of the Analytical Model

After comparing the analytical model result to the experimental data, one deficiency was found in the analytical model at this stage. Because the heat entering the system is constant and according to the conservation of energy equation (3-14), each mass flow rate will result in a different temperature rise in the south side. The analytical model is designed based on an ideal case where there is no recirculation inside the cavity, but this is not the case in the actual experiment. The recirculation affects the total mass flow rate in the TBZ channels. It is difficult to calculate and find the exact effect of recirculation in the system because this effect may fluctuate depending on the gap depth of the TBZ. Therefore, to overcome this problem, an additional term was introduced to the minor losses' equation (3-5) and was dubbed the additional loss coefficient $(K_{add.})$. The minor losses equation then looks like (3-20):

$$h_{lm} = K\frac{v^2}{2g} + K_{add.}\frac{v^2}{2g} \quad (3\text{-}20)$$

This additional loss coefficient covers the general effect of recirculation on the total mass flow rate. The value of the additional loss coefficient can be found based on trial and error for each TBZ gap size. After inputting the experiment's dimensions and conditions, the additional loss coefficient was found to be 22. After applying the additional loss coefficient, the results of the analytical model and the experimental data became close in terms of mass flow rate, temperatures, and amount of heat absorbed by the south side as shown in Table 3-1 and 3-2.

**Table 3-1:** Comparison Between Experiment-1 and Analytical Model Results.

| ***Type of Measurement*** | ***Experimental-1*** | ***Analytical*** | ***Unit*** | ***Difference (%)*** |
|---|---|---|---|---|
| Ambient Temperature ($T_{amb}$) | 27 | 27 | deg. C | 0.0% |
| Room Temperature ($T_R$) | 27 | 27 | deg. C | 0.0% |
| Total Incident Energy ($Q_{inc}$) | 370 | 370 | W/m^2 | 0.0% |
| Heat Flux enter the Room | 65.5 | 61.1 | W/m^2 | 6.7% |
| Heat absorbed by Air in South Side | 44.6 | 50.1 | W/m^2 | 12.3% |
| Net Heat Gain by Air in South Side (q) | 35 | 40.5 | W/m^2 | 15.7% |
| Mass flow Rate ($\dot{m}$) | 6.61E-03 | 6.80E-03 | Kg/s | 2.8% |
| Upper South Temperature ($T_1$) | 40.5 | 41.5 | deg. C | 2.5% |
| Lower South Temperature ($T_4$) | 34.8 | 35.5 | deg. C | 2.0% |
| North Temperature ($T_N$) | 34.5 | 38.2 | deg. C | 10.7% |

**Table 3- 2:** Comparison Between Experiment-2 and Analytical Model Results.

| ***Type of Measurement*** | ***Experimental-2*** | ***Analytical*** | ***Unit*** | ***Difference (%)*** |
|---|---|---|---|---|
| Ambient Temperature ($T_{amb}$) | 24.35 | 24.35 | deg. C | 0.0% |
| Room Temperature ($T_R$) | 24.35 | 24.35 | deg. C | 0.0% |
| Total Incident Energy ($Q_{inc}$) | 370 | 370 | W/m^2 | 0.0% |
| Heat Flux enter the Room | 75.2 | 61.1 | W/m^2 | 18.8% |
| Heat absorbed by Air in South Side | 50.9 | 50.1 | W/m^2 | 1.6% |
| Net Heat Gain by Air in South Side (q) | 37.2 | 40.5 | W/m^2 | 8.9% |
| Mass flow Rate ($\dot{m}$) | 6.89E-03 | 6.85E-03 | Kg/s | 0.6% |
| Upper South Temperature ($T_1$) | 38.31 | 38.78 | deg. C | 1.2% |
| Lower South Temperature ($T_4$) | 32.94 | 32.91 | deg. C | 0.1% |
| North Temperature ($T_N$) | 32.53 | 35.53 | deg. C | 9.2% |

The differences were found to vary between 0.1% to 19%. The differences may have been caused by leaks in the experimental setup. The resulting temperatures in the cavity were very similar in the analytical model to experiment data based on the current mass flow rate, therefore, the decision to calculate the mass flow rate based on the average of Location-2 and Location-3 was optimum. As apparent by the results above, the modification to the analytical model code increased the accuracy of the model's prediction of the effectiveness of the TBZ in life-size building.

## 3.2 Case Studies

The effectiveness of the TBZ is the primary metric in all case studies. The effectiveness is defined as the amount of energy entering the room from the interior wall of north side when TBZ is used compared to when regular insulated wall (3-21). Figure 3-1 illustrates how the effectiveness is calculated.

$$\eta_s = 100\left[\frac{Q_{W/O}-Q_{TBZ}}{Q_{W/O}}\right] \qquad (3\text{-}21)$$

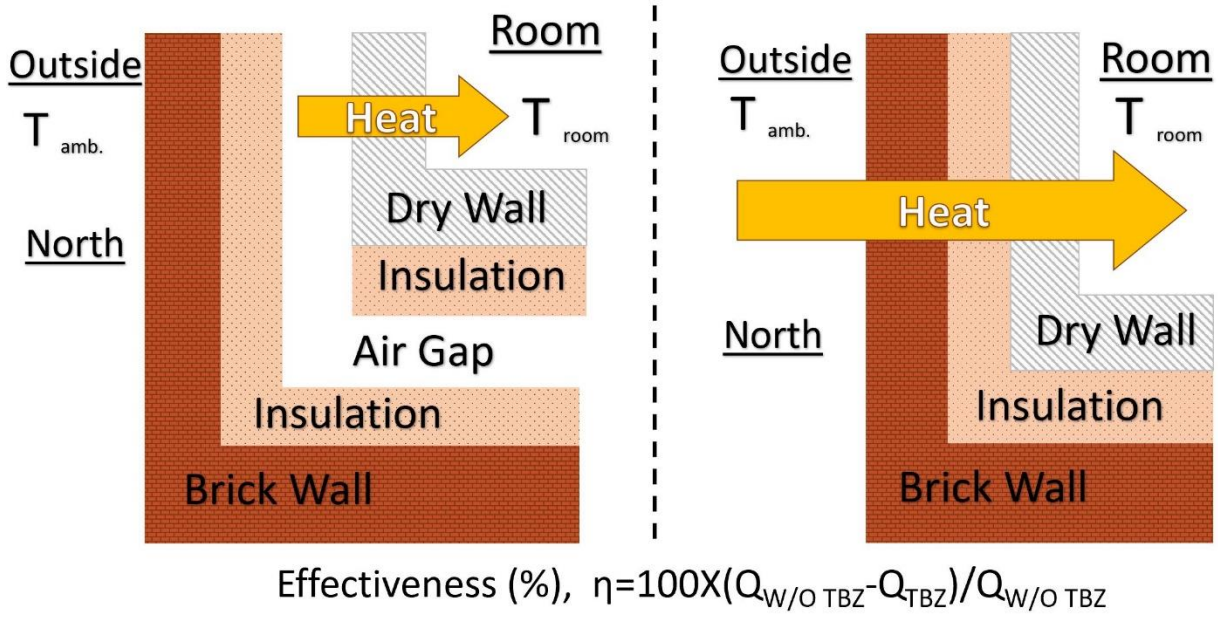


**Figure 3-1:** Demonstration of Calculating the TBZ Effectiveness.

Five cases of a simulated real-life size building in the analytical model will be examined:

1- Cold Climate.
2- Hot Climate.
3- Effect of Insulation.
4- Effect of the fan.
5- Effect of the TBZ gap size.

Since the additional loss coefficient covers the general effect of recirculation, the TBZ gap depths are fixed in the first four cases at the same sizes as in the experimental setup. In the fifth case, it is assumed that the additional loss coefficient is uniform for all the TBZ gap sizes to get an overview of the gap depth effect on the TBZ.

### 3.2.1. Case Study-1: Cold Climate

This study case shows the TBZ effectiveness in a typical building floor in a country with cold weather such as Canada, the United Kingdom, and Germany. The location selected for this case is the city of Ottawa, Canada. The month of January presented the perfect winter month because it is the coldest month of the year with an average daily dry bulb ambient temperature of around -10 ℃ with a standard deviation of 7 degrees. This means that the temperature could reach -17 ℃ during the day (ASHRAE CLIMATIC DESIGN CONDITIONS, 2009). On a clear day in Ottawa, the average daily heat flux was calculated to be around 370 $W/m^2$

based on standard solar resource calculations as seen in Duffie & Beckman (1974).

The building in this case study is 3 m high and has a length and width of 30 m. the TBZ gap size used was the same as experiment's, where the south side was 30 cm and all other sides were 10 cm. The backflow is not highly expected as the ratio of the gap size to the height (B/H) is 0.1, Ryan & Burek (2010). The material of the building is brick (exterior wall) with a brick thickness of 92 mm and a thermal conductivity of 0.6$W/m \cdot K$ (Engineering ToolBox, 2003). The insulation used is Polyisocyanurate which has a thermal conductivity of 0.023 $W/m \cdot K$ (GreenSpec, 2003). The insulation is placed on both sides of the TBZ top and bottom channels while the north channel has insulation in the exterior wall only. This is to increase the amount of heat entering the room from north side of the TBZ system. The insulation thickness is 75 mm. The interior wall was selected to be a dry wall with a thickness of 12.7 mm and thermal conductivity of 0.355 $W/m \cdot K$, Bénichou et al. (2001). There is a clear glass facing ambient temperature and solar-shield grey glass in the interior part of the south side the TBZ channel. The glass thickness is 6 mm with thermal conductivity of 0.8 $W/m \cdot K$, Hochberg et al. (2010). The total wall thickness of the top ceiling is 25.47 cm without the gap and it is 35.47 cm with the TBZ gap. The total wall thickness of the north wall is 17.97 cm without the gap and it is 27.97 cm with the TBZ gap as shown in Figure 3-2.

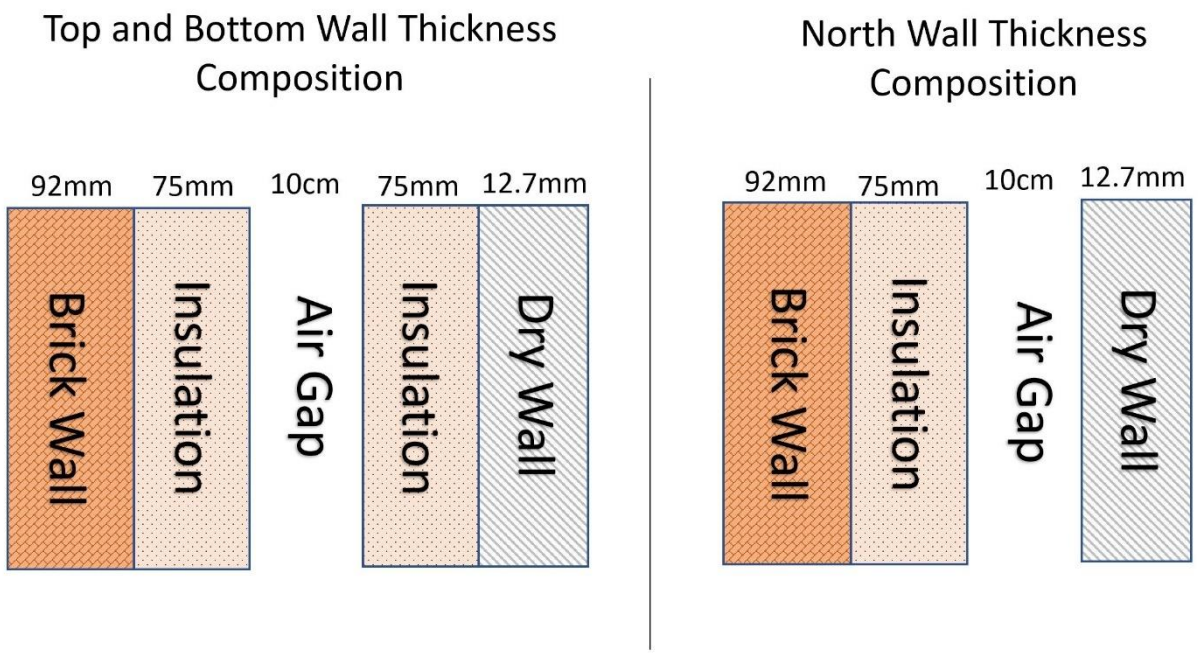


**Figure 3-2:** Wall Thickness Composition With TBZ.

The wall thickness of a building without the TBZ is 22.47 cm which consists of (see Figure 3-3):

1- 92 mm of Brick. 2- 120 mm of insulation. 3- 12.7 mm of drywall.

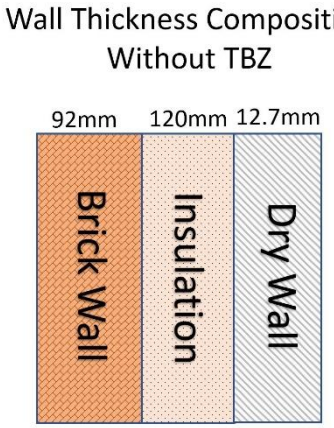


**Figure 3-3:** Wall Thickness Composition Without TBZ.

After taking in the parameters above, the analytical model gave the results shown in Table 3-3

**Table 3-3:** The predicted TBZ effectiveness in Cold Climate.

| ***Type of Measurement*** | ***Cold Climate (Ottawa-CA)*** | ***Unit*** |
|---|---|---|
| Ambient Temperature ($T_{amb}$) | -17 | deg. C |
| Room Temperature ($T_R$) | 24 | deg. C |
| Total Incident Energy ($Q_{inc}$) | 370 | W/m^2 |
| Heat absorbed by Air in South Side | 50.1 | W/m^2 |
| Net Heat Gain by Air in South Side (q) | 3.07E+03 | W |
| Mass flow Rate ($\dot{m}$) | 4.35E-01 | Kg/s |
| Upper South Temperature ($T_1$) | 31.2 | deg. C |
| Lower South Temperature ($T_4$) | 24.1 | deg. C |
| North Temperature ($T_N$) | 25.5 | deg. C |
| Heat Enter to Room from North Side ($Q_{TBZ}$) | 1.18E+02 | W |
| Heat Enter to Room from North Side ($Q_{W/O}$) | -6.64E+02 | W |
| Effectiveness | 117.8 | % |

The result shows clearly the benefit of using the TBZ and the huge amount of energy saved in the building during a very cold winter day. The effectiveness was calculated in this case study to be around 117.8%. The amount of energy that left the building from the north wall without using the TBZ was 662 W. When the TBZ was added to the building, no heat was leaving the room. Instead, about 118 W was entering the room from the TBZ. This is because the temperature in the TBZ north channel was 25.5 ℃, which was more than the room temperature of 24 ℃, and caused the TBZ to supply the room with energy. The temperature reached 25.5 ℃ in the TBZ north channel due to the amount of energy entering from the south side and the insulation in the exterior wall which reduced the amount of heat leaving the TBZ channel to the outside atmosphere.

Therefore, using the TBZ not only reduces the amount of energy leaving the building from the north side, but caused additional heat to enter the building from the TBZ north channel, as seen in this business case.

### 3.2.2. Case Study-2: Hot Climate

This study case focuses on the TBZ effectiveness in a typical building in a country with hot weathers such as Saudi Arabia, Kuwait, and the United Arab Emirates (UAE). The location selected for this case is the city of Dubai. Moreover, Month of August was the perfect summer month because it is the hottest month during the year. During month of August the temperature may exceed 43 ℃ in the

daytime (ASHRAE CLIMATIC DESIGN CONDITIONS, 2009). On a clear day in Dubai, the average daily heat flux was calculated to be around 310 $W/m^2$ based on standard solar resource calculations as seen in Duffie & Beckman (1974).

The case study building is 3 m high and has length and width of 30 m. The TBZ gap size used was the same as the experiment's, where the south side was 30 cm and all other sides were 10 cm. The material of the building is brick (exterior wall) with a brick thickness of 92 mm and a thermal conductivity of 0.6 $W/m \cdot K$ (Engineering ToolBox, 2003). The insulation used is Polyisocyanurate which has a thermal conductivity of 0.023 $W/m \cdot K$ (GreenSpec, 2003). The insulation is placed on both sides of the TBZ top and bottom channels while the north channel has insulation in the exterior wall only. This is to increase the amount of heat entering the room from north side. The insulation thickness is 75 mm. The interior wall was selected to be a dry wall with thickness of 12.7 mm and thermal conductivity of 0.355 $W/m \cdot K$, Bénichou et al. (2001). There is a clear glass facing ambient temperature and solar-shield grey glass in the interior part of the south side of the TBZ channel. The glass thickness is 6 mm with thermal conductivity of 0.8 $W/m \cdot K$ Hochberg et al. (2010). The total wall thickness of the top ceiling is 25.47 cm without the gap and it is 35.47 cm with the TBZ gap. The total wall thickness of the south wall is 17.97 cm without the gap and it is 27.97 cm with the TBZ gap as shown previously in figure-3-2.

The wall thickness of a building without the TBZ is 22.47 cm which consists of (as shown previously in Figure 3-3):

1- 92 mm of Brick. 2- 120 mm of insulation. 3- 12.7 mm of drywall.

After taking in the parameters above, the analytical model gave the results shown in Table 3-4.

**Table 3-4:** The predicted TBZ effectiveness in Hot Climate.

| ***Type of Measurement*** | ***Hot Climate (Dubai-UAE)*** | ***Unit*** |
|---|---|---|
| Ambient Temperature ($T_{amb}$) | 43 | deg. C |
| Room Temperature ($T_R$) | 24 | deg. C |
| Total Incident Energy ($Q_{inc}$) | 310 | W/m^2 |
| Heat absorbed by Air in South Side | 41.9 | W/m^2 |
| Net Heat Gain by Air in South Side (q) | 3.99E+03 | W |
| Mass flow Rate ($\dot{m}$) | 4.28E-01 | Kg/s |
| Upper South Temperature ($T_1$) | 34.6 | deg. C |
| Lower South Temperature ($T_4$) | 25.4 | deg. C |
| North Temperature ($T_N$) | 27.9 | deg. C |
| Heat Enter to Room from North Side ($Q_{TBZ}$) | 2.99E+02 | W |
| Heat Enter to Room from North Side ($Q_{W/O}$) | 3.07E+02 | W |
| Effectiveness | 2.5 | % |

The results show very small saving in energy by using the TBZ in the building. The effectiveness was calculated in this case study to be around 2.5%. The amount of energy that entered the building from the north wall without using the TBZ was 307 W. After adding the TBZ to the building, the amount of energy that entered the building from north wall was 299 W. Moreover, the temperature in the TBZ north channel was 27.9 ℃ which is more than the room temperature of 24 ℃, and caused energy to go from the TBZ to the room. In addition to the very small energy saving by the TBZ in the north side of the building, the temperature in the south side channel had been reduced due to the low temperature air that comes from the TBZ north side. This made the south side temperature vary between 25.4 ℃ to 34.6 ℃, which has the effect of reducing the amount of heat entering the south side, meaning less cooling demand difference between south and north.

One explanation of the TBZ's poor energy saving in this case is the absence of insulation in the interior channel in the north side of the TBZ. The interior insulation could reduce the heat entering the building from the north side. Even so, the TBZ temperature reduction in the south side could reduce the differencing in the cooling load between south and north sides of the building.

### 3.2.3. Case Study-3: Effect of Insulation

In the two previous case studies the interior wall of the building in the north side had no insulation. This case study will demonstrate the effect of adding insulation

to the TBZ interior channel in the north side. All other material properties, dimensions, temperatures and heat flux will be the same as they were in case studies one and two.

#### 3.2.3.1. Insulation effect in Cold Climate

After inputting the same parameters as in Case Study-1 in addition to the insulation in the interior wall in the north side, the results were as shown in Table 3-5.

**Table 3-5:** The Effect of Insulation in the TBZ effectiveness in Cold Climate.

| ***Type of Measurement*** | ***Insulation (Ottawa-CA)*** | ***No Insulation (Ottawa-CA)*** | ***Unit*** |
|---|---|---|---|
| Ambient Temperature ($T_{amb}$) | -17 | -17 | deg. C |
| Room Temperature ($T_R$) | 24 | 24 | deg. C |
| Total Incident Energy ($Q_{inc}$) | 370 | 370 | W/m^2 |
| Heat absorbed by Air in South Side | 50.1 | 50.1 | W/m^2 |
| Net Heat Gain by Air in South Side (q) | 3.07E+03 | 3.07E+03 | W |
| Mass flow Rate ($\dot{m}$) | 4.32E-01 | 4.35E-01 | Kg/s |
| Upper South Temperature ($T_1$) | 31.3 | 31.2 | deg. C |
| Lower South Temperature ($T_4$) | 24.2 | 24.1 | deg. C |
| North Temperature ($T_N$) | 25.6 | 25.5 | deg. C |
| Heat Enter to Room from North Side ($Q_{TBZ}$) | 33.1 | 1.18E+02 | W |

| | | | |
|---|---|---|---|
| Heat Enter to Room from North Side ($Q_{W/O}$) | -6.64E+02 | -6.64E+02 | W |
| Effectiveness | 105.0 | 117.8 | % |

Table 3-5 shows that using insulation reduced the effectiveness of the TBZ from 117.8% to 105%. A reduction of 12.8% is something to consider when it comes to energy saving. On the other hand, insulation could provide additional benefits in the night by reducing the energy escaping from the north side of the building in addition to the significant energy saving during the day. The decision to use the north side interior insulation would depend on the type of the building and if there are occupants during the nights.

#### 3.2.3.2. Insulation effect in Hot Climate

After inputting the same parameters as in Case Study-2 (Hot Climate) in addition to the insulation in the interior wall in the north side, the results were as shown in Table 3-6.

**Table 3- 6:** The Effect of Insulation in the TBZ effectiveness in Hot Climate.

| ***Type of Measurement*** | ***Insulation (Dubai-UAE)*** | ***No Insulation (Dubai-UAE)*** | ***Unit*** |
|---|---|---|---|
| Ambient Temperature ($T_{amb}$) | 43 | 43 | deg. C |
| Room Temperature ($T_R$) | 24 | 24 | deg. C |
| Total Incident Energy ($Q_{inc}$) | 310 | 310 | W/m^2 |
| Heat absorbed by Air in South Side | 41.9 | 41.9 | W/m^2 |

| | | | |
|---|---|---|---|
| Net Heat Gain by Air in South Side (q) | 3.97E+03 | 3.99E+03 | W |
| Mass flow Rate ($\dot{m}$) | 4.20E-01 | 4.28E-01 | Kg/s |
| Upper South Temperature ($T_1$) | 34.9 | 34.6 | deg. C |
| Lower South Temperature ($T_4$) | 25.5 | 25.4 | deg. C |
| North Temperature ($T_N$) | 28.1 | 27.9 | deg. C |
| Heat Enter to Room from North Side ($Q_{TBZ}$) | 83.9 | 2.99E+02 | W |
| Heat Enter to Room from North Side ($Q_{W/O}$) | 3.07E+02 | 3.07E+02 | W |
| Effectiveness | 72.7 | 2.5 | % |

Table 3-6 shows that using insulation significantly increases the effectiveness of the TBZ from 2.5% to 72.7%. Moreover, the insulation will prevent the energy from entering the building during the night.

### 3.2.4 Case Study-4: Effect of Fan

One of the ideas to increase the TBZ effectiveness is to introduce a fan into the TBZ system to increase the mass flow rate in the TBZ channel. Introducing the fan in the system will increase the pressure in the cavity and may reduce the natural convection loop in the middle of south side cavity. This will increase the mass flow rate which will result in more energy/heat transferred from the hot side to the cold side. To form an idea about how much driving pressure is produced by the TBZ to

be able to transfer the air from south to north and vise-versa naturally. The amount of driving pressure will vary based on the gap size and amount of energy absorbed into the air, the driving pressure calculated in Case Study-1 was 0.77 Pa. Therefore, a fan with pressure of 0.5 Pa, 1.0 Pa, 3 Pa, 5 Pa and 10 Pa will be studied. This case study examines two major factors: The first one is the effectiveness of the TBZ, the second one is the net additional power delivered by the fan (3-22) which is defined as the difference between the amount of additional power delivered to the system by the fan and the amount of power consumed by the fan.

$$Net\ Additional\ Power\ Delivered\ = \\ Additional\ Power\ Delivered\ - Power\ Consumed \qquad (3\text{-}22)$$

This is to make sure that the TBZ system is not losing more energy by using the fan. The fan efficiency was chosen to be at 85%. This case study will be applied for only cold climate with insulation (Case Study-3) and without insulation (Case Study-1).

The analytical model had been adjusted to allow additional pressure from external source such as fan. the program calculates both the total energy delivered to the room with support of fan and the energy consumed by the fan. The input into the analytical model for this case study is identical to Case Study-1 and Case Study-3 in addition to the various pressure levels of the fan. The same previous material properties, dimensions, temperatures and heat flux will be used. The

effectiveness of the TBZ increased in both scenario with and without insulation as shown in Figure 3-4.

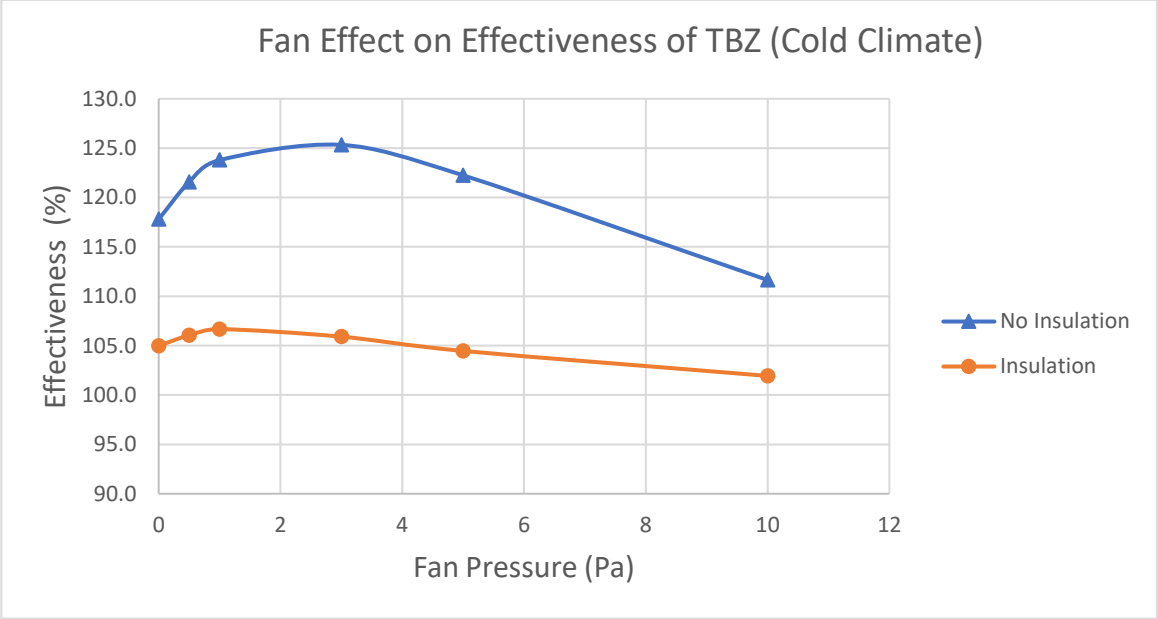


**Figure 3-4:** Fan Effect on Effectiveness of TBZ in Cold Climate.

The effect was much clearer in the absence of insulation where the effectiveness increased from 117.8% without fan to 125% with a fan that has pressure of 3.0 Pa. This increase is due to the increase of both mass flow rate from $43.5 \times 10^{-2}\ Kg/s$ to $90.6 \times 10^{-2}\ Kg/s$ and the north side temperature from 25.5 ℃ to 25.7 ℃. Although the mass flow rate increased 1.61 $Kg/s$ with higher pressure fan (10 Pa), the temperature in the north side actually decreased to 24.5 ℃. With a fan that has pressure of 1.0 Pa, the north side temperature was 26.0 ℃ but the effectiveness still did not exceed 124% which is due to the low mass flow rate of

$62.3 \times 10^{-2}\ Kg/s$. The right combination of high temperature and mass flow rate achieves the maximum TBZ effectiveness possible. To make sure that fan is not using more energy than it delivered, the net additional power delivered by fan was plotted against Fan pressure in Figure 3-5.

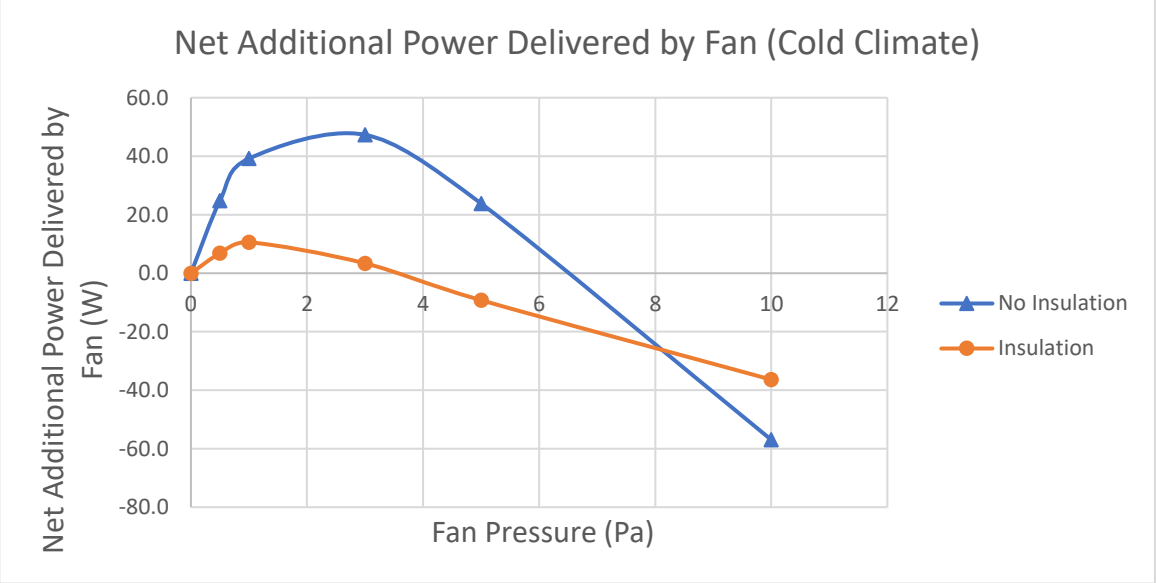


**Figure 3-5:** Net Additional Power Delivered by Fan in Cold Climate.

The no insulation scenario in Figure 3-5 showed that using a fan with 3 Pa pressure would save the maximum additional energy from the fan compared to other values. By checking both effectiveness and the net additional power delivered by fan, we can conclude that using 3 Pa pressure fan would be the optimum solution for the no insulation scenario (Case Study-1).

By checking both effectiveness and the net additional power delivered by fan for the insulation case scenario, we found that the optimum solution is to use a fan

with 1 Pa pressure. In contrast, the amount of energy saved in the with-insulation scenario may not be significant if the initial and operation cost of the fan is greater than the cost saving by the net additional power delivered by the fan.

### 3.2.5. Case Study-5: Effect of the TBZ Gap size

This case study examines the effect of the TBZ gap size on the effectiveness of the TBZ. The problem is that additional loss coefficient ($K_{add.}$) is known for experiment's gap size, but not for the other gap sizes. For that reason, it is assumed that the different gaps would have a uniform additional loss coefficient ($K_{add.}$) to be able to run the analytical model and give a general overview of how the effectiveness of the TBZ would react to the changing the gap size.

The only TBZ gap size that would be changing in the south side gap. All other gaps were kept to 10 cm width. We will examine the gap size from 5 cm to 50 cm. All other input of this case study is identical to case studies-1 and 3. The same material properties, dimensions, temperatures and heat flux will be used. This case study will be applied for cold climate with-insulation and without-insulation.

After inputting the updated data into the analytical model for the cold climate, the effect of the gap size on the TBZ system is plotted in Figure 3-6.

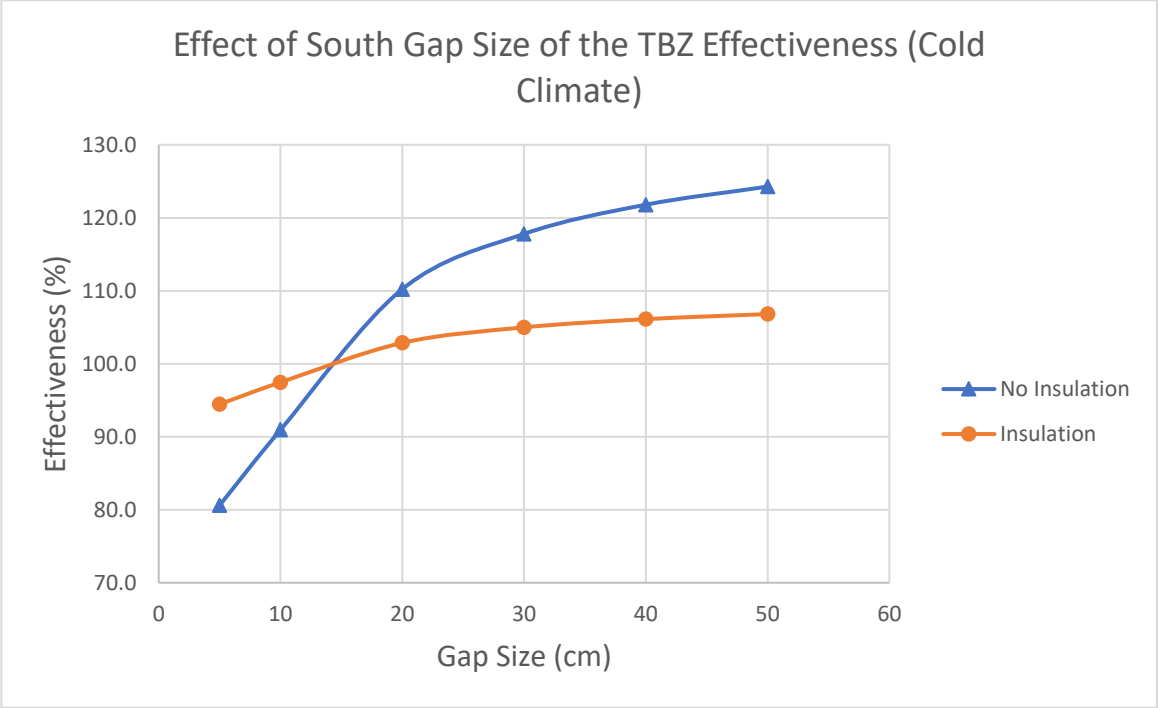


**Figure 3-6:** Effect of South side Gap Size of the TBZ Effectiveness (Cold Climate)

Both with-insulation and without-insulation cases showed significant increase in the TBZ effectiveness when the gap size increased from 5 cm to 20 cm. Beyond the 20 cm gap size, both of scenarios showed slight increase in the effectiveness as the gap size increased from 30 cm to 50 cm. In addition, the room was losing energy in both cases at gap sizes 5 cm and 10 cm.

Additionally, another assumption made is that the gap size of the south, north, top and bottom sides will be uniform. We will examine the gap size from 5 cm to 50 cm. All other input of this case study is identical to case studies one and three. The same material properties, dimensions, temperatures and heat flux will be used.

This case study will be applied for cold climate with-insulation and without-insulation.

After inputting the updated data into the analytical model for the cold climate, the effect of the gap size on the TBZ system is plotted in Figure 3-7.

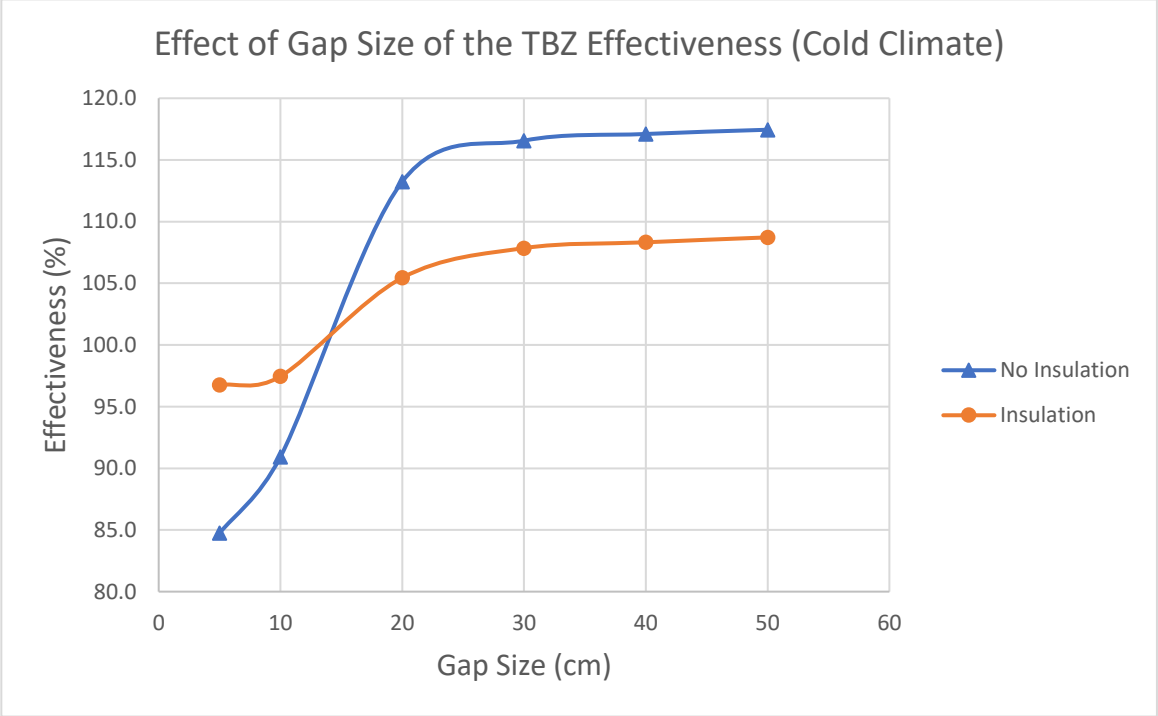


**Figure 3-7:** Effect of Uniform Gap Size of the TBZ Effectiveness (Cold Climate)

Both with-insulation and without-insulation cases showed significant increase in the TBZ effectiveness when the gap size increased from 5 cm to 30 cm. Beyond the 30 cm gap size, both of scenarios became almost plateaus in the effectiveness

as the gap size increased from 30 cm to 50 cm. In addition, the room was losing energy in both cases at gap sizes 5 cm and 10 cm

By comparing the result of the 30 cm gap size in this case study with Case Study-1, we note that the results are very close and this is due to the gap size similarity in the south side where it allows the air to gain more energy before transferring it to the north side. Moreover, Case Study-1 is much more realistic and easier to construct in regular real-life size building.

# Chapter 4

# 4. Summary and Conclusion

## 4.1 Summary of the Research Work

This study investigated the effectiveness of the TBZ in a real building. Most of the literature reviewed for this study had experiments on open systems and the ones on closed systems had no overall correlations between the different parameters affecting the TBZ. Such parameters are necessary for running a year-long analysis of the TBZ's effectiveness in a building. Therefore, an analytical model was developed using MATLAB to predict the effectiveness of TBZ after including the parameters that could impact the results. The analytical model was validated using experimental data. Due to the recirculation, the mass flow rate was not calculated accurately; therefore, an additional loss coefficient was added to the analytical model to counteract the effect of the recirculation. After calculating the additional loss coefficient value that correlated with experimental setup gap size, the model produced accurate predictions. The predicted temperatures had reasonable accuracy when verified using the experiment results. The additional loss coefficient value was assumed to be the same in the experiment and the life-size building as long as they had the same TBZ gap width associated with that coefficient value. Based on this assumption, the effectiveness of TBZ in a real building was examined in very cold climate and very hot climate conditions as simulated in the analytical model. The TBZ showed more then 115% effectiveness

in cold climate compared to regular walls with insulation. Meanwhile, it showed a very small effectiveness of 2.5% in very hot climate conditions. The addition of insulation to the north wall reduced the effectiveness of TBZ in cold climate to 105%, but caused it to jump to 72% in very hot climate conditions. Following that, and with the knowledge that pumping air in an HVAC system consumes much less energy than heating it, a fan was added to the TBZ system to examine the impact it would have on its effectiveness. In Case Study-4, the analytical model showed that a fan with a pressure of 3 Pa provided the optimum result which is an increase of 7.5% in the effectiveness of the TBZ with the dimensions stated in the case study. Lastly, the effect of the TBZ gap size was examined in an experiment which showed that the effectiveness will increase with the gap width until the gap is 30 cm wide. After that point the effectiveness plateaus and does not increase with the gap width.

## 4.2 Conclusions

Based on the analytical model, the presence of TBZ in a life-size building would result in a significant reduction in the heat load in the north side and redistribution the heat via the channels surrounding the building, which will act as additional insulation. The TBZ actually enhanced the thermal resistance of the building envelope. Moreover, the amount of heat that enters to the south side would be reduced markedly, and a fan can contribute positively to the redistribution of heat in TBZ and increase its effectiveness. All these benefits shown in experiment

results and the analytical model results of different case studies support the claim that a TBZ would reduce the building's consumption of energy from non-renewable sources. Moreover, the analytical model can assist the HVAC engineers to reduce the loads needed by the system and calculate for them the amount of heat entering the building from each side by the TBZ.

One of the advantages of TBZ is that it is integrated into the building and does not require the assistance of another system the way SAW requires an HVAC system. TBZ heats the building independently of ventilation unlike Solar Window which works through ventilating the building. However, it is likely that TBZ will be applied to the design of new buildings, not added to existing buildings due to the nature of this method which requires it to permeate the walls and floors of the building and therefore should be installed during the construction stage.

## 4.3 Recommendation and Future Work

It is always good to remember that the ultimate goal is to reach NZEB by producing more renewable energy and reducing the building's needs for energy from non-renewable sources. The current study focused on reducing the energy consumed by buildings through a passive heating approach. TBZ was the method selected from among the different passive heating approaches. The implementation of the TBZ in the building showed significant results. Simulations

of cold climates showed that the TBZ can achieve an effectiveness of about 115%. These promising results encourage further research to be conducted on TBZ.

The most important component in any system that utilizes the solar energy is the optical properties of the glass parts. There is a wealth of knowledge regarding the optical properties of the glazing of flat plate solar collectors as they are heavily researched. If used in the design and optimization of Solar Thermal Buffer Zones, this knowledge results in glazing with optimal optical properties that would minimize heat loss through radiation and conduction. This leaves the problem of minimizing heat loss inside the cavity through convection to the exterior glass and the uncontrollable weather outside.

A solution can be attempted by inserting intermediate highly absorptive glass panels in the middle of the south side channel between the exterior and interior glass panels. This may allow for more utilization of the solar energy due to the fact that the radiation from the intermediate glass panels would be inside the cavity. This could transfer more energy to the air which could increase the effectiveness of the system. The number of intermediate panels can be adjusted until optimal results are achieved.

A fully controlled environment housing the TBZ experiments would enable more in-depth study of the effect of the TBZ through changing the ambient temperature to mirror that of different seasons, different times of day, and different internal temperatures of the TBZ. A full-year simulation would provide a complete

picture of the impact of TBZ on the total energy consumption, and could reveal the suboptimal conditions where the TBZ fan would consume more energy than the TBZ is saving in optimal conditions.

The dependency of the mass flow rate on the B/H aspect ratio was not observed in the analytical model, but it was observed in previous experimental work. The additional loss coefficient in the analytical model may vary depending on the TBZ gap B/H aspect ratio. The analytical model predicts the mass flow rate based on the additional loss coefficient value. To enhance the estimation of the mass flow rate in different gap sizes, multiple experiments have to be conducted with different B/H aspect ratios. Furthermore, the additional loss coefficient value must be adjusted in the analytical model until accurate temperature results are produced. Through this empirical method, a relationship may be identified between the additional loss coefficient (used to find the mass flow rate in analytical model) and the B/H aspect ratio. Integrating this relationship into the analytical model would improve prediction accuracy.

# Appendices

## 5.1 Appendix A - Velocity Measurement Conversion

The conversion from voltage to velocity is based on the Log Square transfer function.

$$LSQ = ln^2(1 + gV)$$

Where $g$ is the gain factor optimized for a specific probe type. For the omnidirectional probe, $g$ is set as 150.

$$LSQ = A_0 + A_1 e + A_2 e^2 + A_3 e^3 + \ldots$$

Where $A$ values are found from the manufacturer provided calibration, and $e$ is the measured voltage. The resulting equation can then be written.

$$V_e = \left[exp((A_0 + A_1 e + A_2 e^2 + A_3 e^3 + \ldots)^{1/2})\right]/g$$

The pressure is then accounted for by the following.

$$V_p = V \frac{p}{101.325\ kPa}$$

Where $p$ is the measured atmospheric pressure. The correction for humidity and temperature is finally applied.

$$V = V_p[1 + f(r \times f(T))]$$

Where $f$ is a manufacturer provided calibration function for the respective values, $r$ is the relative humidity and $T$ is the measured temperature. This will result in an instantaneous velocity reading. To account for the turbulent nature of the flow

many in instantaneous voltage readings need to be taken, and converted to velocity, then averaged to get a mean velocity reading at that location.

## 5.2 Appendix B – Pyranometer Readings

Multiple measurements were taken to observe the effect of glass and distance in reducing the amount of heat flux entering the building. Different table showed different scenarios between Table 5-1 through Table 5-4

**Table 5-1:** Glass Plates Affect on the Heat Flux with Distance of 1.38 m.

| Type of Measurement | Distance from illumination (m) | Heat Flux (W/m^2) | |
|---|---|---|---|
| | | Experiment-1 | Experiment-2 |
| Heat Flux in Front of Exterior Glass | 1.38 | 369.8 | 370.5 |
| Heat Flux Behind Interior Glass | 1.38 | 99.0 | 99.00 |
| Percentage of Heat Flux Reduction Due to Glass Plates | | 73.23 | 73.28 |

**Table 5-2:** Glass Plates Affect on the Heat Flux with Distance of 1.70 m.

| Type of Measurement | Distance from illumination (m) | Heat Flux (W/m^2) | |
|---|---|---|---|
| | | Experiment-1 | Experiment-2 |
| Heat Flux in Front of Exterior Glass | 1.70 | 262.4 | 262.4 |
| Heat Flux Behind Interior Glass | 1.70 | 65.7 | 75.20 |
| Percentage of Heat Flux Reduction Due to Glass Plates | | 74.96 | 71.34 |

**Table 5- 3:** Distance Affect on the Heat Flux without Glass Plates

| Type of Measurement | Distance from illumination (m) | Heat Flux (W/m^2) | |
|---|---|---|---|
| | | Experiment-1 | Experiment-2 |
| Heat Flux in Front of Exterior Glass | 1.38 | 369.8 | 370.5 |
| Heat Flux in Front of Exterior Glass | 1.70 | 262.4 | 262.4 |
| Percentage of Heat Flux Reduction Due to Distance | | 29.04 | 29.18 |

**Table 5- 4:** Distance Affect on the Heat Flux with Glass Plates

| Type of Measurement | Distance from illumination (m) | Heat Flux (W/m^2) | |
|---|---|---|---|
| | | Experiment-1 | Experiment-2 |
| Heat Flux Behind Interior Glass | 1.38 | 99.0 | 99.00 |
| Heat Flux Behind Interior Glass | 1.70 | 65.5 | 75.2 |
| Percentage of Heat Flux Reduction Due to Distance | | 33.84 | 24.04 |

Table 5-1 and 5-2 showed the glass plates responsible for reducing around 73% of the heat flux. Part of this amount of heat flux absorbed by the glass plates and air where the other part had been reflected dissipated by the glass plates. Table 5-3 and 5-4 showed the distance between the two plates of glass was responsible for reducing around 29% of the heat flux coming from blackbody.

# References

Afonso, C., & Oliveira, A. (2000). Solar chimneys: simulation and experiment. *Energy and Buildings, 32*(1), 71-79.

Ardiani, N. A., & Koerniawan, M. (2017). Glass and perforated metal double skin facade performance in hot humid climate. *DIMENSI, 44*(2), 143-148.

Arons, D. M. (2000). *Properties and Applications of Double-Skin Building Facades.* Cambridge: Massachusetts Institute of Technology.

ASHRAE CLIMATIC DESIGN CONDITIONS. (2009). *ASHRAE CLIMATIC DESIGN CONDITIONS*. (Ashrae meteo.info) Retrieved from http://ashrae-meteo.info/#

Ayinde, T., Said, S., & Habib, M. (2006). Experimental investigation of turbulent natural convection flow in a channel. *Heat and Mass Transfer, 42: 169*(3).

Bénichou, N., Sultan, M., MacCallum, C., & Hum, J. (2001). *Thermal properties of wood, gypsum and insulation at elevated temperatures.* National Research Council Canada.

Bouchair, A. (1994). Solar chimney for promoting cooling ventilation in southern Algeria . *Building Services Engineering Research and Technology, 15*(2), 81 - 93.

Chen, Z., Bandopadhayay, P., Halldorsson, J., Byrjalsen, C., Heiselberg, P., & Li, Y. (2003). An experimental investigation of a solar chimney model with uniform wall heat flux. *Building and Environment, 38*(7), 893-906.

Duffie, J., & Beckman, W. (1974). *Solar energy thermal processes.* New York, NY: John Wiley and Sons.

Engineering ToolBox. (2003). *Thermal Conductivity of common Materials and Gases*. Retrieved from Engineering ToolBox: https://www.engineeringtoolbox.com/thermal-conductivity-d_429.html

Figliola, R., & Beasley, D. (2000). *Theory and Design for Mechanical Measurements.* John Wiley & Sons, Inc.

Fiuk, J. J., Dutkowski, K., & Piatkowski, P. (2017). An experimental study on the Thermal Efficiency of a Passive Solar Air Collector. *Engineering Transactions, 65*(2), 251-268.

Friedrich, K. (2011). *Experimental and Numerical Investigation of Solar Airflow Windows.* Hamilton, ON.

GreenSpec. (2003). *Insulation materials and their thermal properties*. Retrieved from GreenSpec: http://www.greenspec.co.uk/building-design/insulation-materials-thermal-properties/

Habib, M., Said, S., Ahmed, S., & Asghar, A. (2002). Velocity characteristics of turbulent natural convection in symmetrically and asymmetrically heated vertical channels. *Experimental Thermal and Fluid Science, 26*(1), 77-87.

Hochberg, A., Hafke, J.-H., & Raab, J. (2010). *Open I Close: Windows, Doors, Gates, Loggias, Filters.* Birkhäuser.

International Energy Agency. (2010). *Buildings Overview*. Retrieved from International Energy Agency: https://www.iea.org/etp/buildings/dataandfigures/buildingsoverview/

International Energy Agency. (2017). *Buildings*. Retrieved from International Energy Agency: https://www.iea.org/buildings/

Jan, A., Hamed, M., Razaqpur, G., & Foo, S. (2014). *Investigation of the Use of Solar Thermal Buffer Zone in Buildings.* (I. Dincer, A. Midilli, & H. Kucuk, Eds.) In: Progress in Exergy, Energy, and the Environment (pp. 841-848): Springer, Cham.

La Pica, A., Rodono, G., & Volpes, R. (1993). An Experimental Investigation on natural convection of air in a vertical channel. *International Journal of Heat and Mass Transfer, 36*(3), 611-616.

Natural Resources Canada. (2018). *Comprehensive Energy Use Database*. Retrieved from Natural Resources Canada: http://oee.nrcan.gc.ca/corporate/statistics/neud/dpa/menus/trends/comprehensive_tables/list.cfm

Onbasioglu, H., & Egrican, A. (2002). Experimental approach to the thermal response of passive systems. *Energy Conversion and Management, 43*(15), 2053-2065.

Richman, R., & Pressnail, K. (2009). A more sustainable curtain wall system: Analytical modeling of the solar dynamic buffer zone (SDBZ) curtain wall. *Building and Environment, 44*(1), 1-10.

Richman, R., & Pressnail, K. (2010). Quantifying and predicting performance of the solar dynamic buffer zone (SDBZ) curtain wall through experimentation and numerical modeling. *Energy and Buildings, 42*(4), 522-533.

Ryan, D., & Burek, S. (2010). Experimental study of the influence of collector height on the steady state performance of a passive solar air heater. *Solar Energy, 84*(9), 1676-1684.

Saifi, N., Settou, N., Dokkar, B., Negrou, B., & Chennouf, N. (2012). Experimental study and simulation of airflow in solar chimneys. *Energy Procedia, 18*, 1289-1298.